Stable force control and contact transition of a single link flexible robot using a fractional-order controller

Feliu-Talegon, Daniel; Feliu-Batlle, Vicente; Tejado, Inés; Vinagre, Blas M.; Hossein Nia Kani, Hassan

DOI
10.1016/j.isatra.2018.12.031

Publication date
2019

Document Version
Accepted author manuscript

Published in
ISA Transactions

Stable force control and contact transition of a single link flexible robot using a fractional-order controller☆

Daniel Feliu-Talegon, Vicente Feliu-Batlle, Inés Tejado, Blas M. Vinagre, S. Hassan HosseinNia

Abstract

The control of robots that interact with the environment is an open area of research. Two applications that benefit from this study are: the control of the force exerted by a robot on an object, which allows the robot to perform complex tasks like assembly operations, and the control of collisions, which allows the robot safely collaborate with humans. Robot control is difficult in these cases because: 1) bouncing between free and constrained motion appears that may cause instability, 2) switching between free motion (position) controller and constrained motion (force) controller is required being the switching instants difficult to know and 3) robot control must be robust since the mechanical impedance of the environment is unknown. Robots with flexible links may alleviate these drawbacks. Previous research on flexible robots proved stability of a *PD* controller that fed back the motor position when contacting an unknown environment, but force control was not achieved. This paper proposes a control system that combines a fractional-order *D* tip position controller with a feedforward force control. It attains higher stability robustness and higher phase margin than a *PD* controller, which is the integer-order controller of similar complexity. This controller outperforms previous controllers: 1) it achieves force control with nearly zero steady state error, 2) this control is robust to uncertainties in the environment and motor friction, 3) it guarantees stability (like others) but it also guarantees a higher value of the phase margin, i.e., a higher damping, and a more efficient vibration cancellation, and 4) it effectively removes bouncing. Experimental results prove the effectiveness of this new controller.

Keywords: force control, flexible robots, fractional-order control, hybrid systems control, robust control

1. Introduction

The efficient control of the interaction of robots with the environment broadens the range of application of robotics. Two applications that are benefited from this are: force control, which allows the robot to perform complex tasks like assembly operations, and collision control, which allows the robot to safely collaborate with humans.

The control of a robot interacting with the environment is difficult because: 1) bouncing between free and constrained motion appears that may cause instability, 2) switching between a free motion (position) controller and a constrained motion (force) controller is required being the switching instants difficult to obtain, and 3) robot control must be robust since the mechanical impedance of the environment is unknown.

Flexible robots are characterized by having at least one flexible element in its mechanical configuration. Flexible links are mostly utilized because they allow for robot designs with reduced weight, which involves some significant advantages over standard rigid robots: a lightweight flexible robot can perform faster movements than its equivalent in dimensions rigid counterpart, it is more easily transportable, its energy consumption is lower, and its payload-to-arm weight ratio is higher (see e.g. [1]).

Interaction with the environment is better dealt by flexible robots than by standard rigid robots, e.g, in force control tasks [2] or in cooperative tasks with humans [3]. The following advantages can be ascertained in the case of flexible link robots:

1. When a rigid robot and a rigid object collide, the contact force grows very quickly (in μs), reaching a very high value before the control system acknowledges the contact. Then, the object or a robot component may be broken. When a flexible link collides, instead, part of its kinetic energy is gradually transformed into link elastic potential energy. The contact force grows then more slowly (in *ms*) and the control system can timely detect the impact and switch from position to force control, reducing the harming effects of the impact.
2. When a rigid robot performs tasks involving contact with the environment, like assemblies, small errors in the robot end effector position yield high contact forces that often impede the execution. This is overcome using complex sensory systems, computer-aided design models of the environment and complex task

planning systems. Instead, flexible link robots absorbe these errors by slightly deforming their links, yielding moderate values of the contact force that facilitate these tasks. This deflecting feature has been exploited in industry, in which compliant mechanisms are inserted at certain points of the robot to achieve assembly tasks, e.g., the Remote Center of Compliance Device [4].

3. Impedance control is a useful technique that combines position-force control in robotics [5], being quite stable in transitions from free to constrained movements. It can be easily implemented using robots with flexible links, in which part of the impedance control is passively performed by the compliant structure of the robot.
4. Damage on an operator of the impact of a robot would be drastically reduced. For example, the head injury criterion HIC [3], [6] is defined as:

$$HIC = 2\left(\frac{2}{\pi}\right)^{\frac{3}{2}}\left(\frac{K_{cov}}{M_{oper}}\right)^{\frac{3}{4}}\left(\frac{M_{rob}}{M_{rob}+M_{oper}}\right)^{\frac{7}{4}} v_{rob}^{\frac{5}{2}} \tag{1}$$

where v_{rob} is the speed of the robot, M_{rob} is the mass of the robot, M_{oper} is the mass of the impacted operator, and K_{cov} is the lumped stiffness of a compliant cover on the arm (in our case, it is assimilated to the compliance of the flexible link). HIC index is much smaller in a flexible link robot than in a rigid one because M_{rob} and K_{cov} are smaller. Moreover, control systems can be designed taking into account previous issues 1) to 3) to further reduce collision harm.

However, undesired vibrations and deflections appear in the structure of flexible link robots that make their control significantly complicate. A survey on free motion control techniques of these robots is [7].

Several strategies were proposed to control rigid robots interacting with the environment. They can be grouped into impedance control [8] and hybrid position-force control [9], and have also been extended to flexible robots. Examples for robots with two flexible links are impedance control [10] and hybrid position-force control [11].

Research has been carried out on contact detection mechanisms for rigid robots [12], [13] and flexible link robots [14]. Thresholds of some functions of generalized robot momenta and motor torques were used to trigger the change of the control law. In these control systems, after the contact had been detected, the robot was stopped in

a position in which no contact was established with the object (preventing harming a person) or in a position in which some force was exerted on a soft object. In all these cases, rebounds were minimum and did not deteriorate the control performance.

Control of rigid robots interacting with the environment has been proposed, that switches from position to force control in function of a contact detection mechanism, e.g., [15]. However, these robots had to approach the object slowly because of the above mentioned problems. One of the first applications of this kind of controllers to single link flexible robots was [16]. This controller was later extended to a two links - three degrees of freedom [1] (DOF) flexible robot in [18], in which a hybrid position-force control combined with a collision detection algorithm was developed. These flexible robots could approach faster to the object. Contact detection mechanisms for flexible link robots were proposed that switched between controllers [19] or between references for a given controller [2]. The second controller was more robust than the first but less efficient. In [20], a contact detection mechanism was combined with a force control of two flexible fingers of a gripper of a 6 DOF manipulator in order to manipulate fragile objects. Finally, [21] described a hybrid position-force control of a sensing antenna that slides on a surface and recognizes an object by repetitive control. In all these works, rebounds may appear in the collision. Moreover, control robustness when contacting objects of unknown rigidity has not been addressed in most of them.

Previous methods switched controllers only once: the first time that the robot changed from free to constrained motion. If subsequent rebounds appeared, the control law was not varied (with the exception of [15] in which the contact detection mechanism remained ever active, switching controllers in the rebounds). Then robust asymptotic stability is required in the rebounds. Moreover, control should be robust to the unknown impedance of the collided object. In [22], the stability of a *PD* controller of a single link flexible robot that fed back the motor position in the case of rebounds with an unknown environment was proven, but force control was not achieved. Moreover, controlling motor position is not as efficient in removing vibrations of a flexible link as

[1] The number of degrees of freedom that a manipulator possesses is the number of independent position variables which would have to be specified in order to locate all parts of the mechanism (see e.g. [17]). In the case of a flexible link manipulator it has to be also specified that external forces would not be applied.

controlling tip position or the moment at certain points of the link.

We address the control of a single link flexible robot that has to exert a programmed force on an object. A fractional-order D tip position controller is combined with a feedforward position/force control. It cancels link vibrations better than [22] because it controls the tip position, which is clearly affected by link vibration, unlike the mentioned work that controls the motor position, which barely reflects link vibration. Moreover, the proposed control system attains higher stability robustness and phase margin than a PD tip position controller, which is the integer-order controller of complexity similar to the proposed one. Our control system also attains force control with nearly zero steady state error and is robust to nonlinear joint friction.

Fractional-order operators have been used to implement robust controllers. Applications to damping vibrations on flexible links are: a fractional-order proportional-derivative control (FPD) of the attitude of a flexible spacecraft [23]; controls that include proportional and two fractional-order derivative terms of different orders for a planar two degrees of freedom flexible robot [24]; a FPD for a single link flexible robot robust to payload changes [25]; and a fractional-order proportional-integral controller for a flexible link implemented by an analog device denoted fractor [26].

Fractional-order hybrid position-force control of a rigid robot with compliant joints has been studied in [27]. Fractional-order controllers were also used in cooperation tasks between two manipulators with compliant joints in [28]. Our paper addresses for the first time the fractional-order force control of flexible link robots in contact tasks, that is robust to rebounds, environment uncertainties and joint friction.

Asymptotic stability in the case of rebounds is guaranteed by using a recent result on hybrid fractional-order systems developed in [29]. Robustness to joint friction is achieved by implementing a two nested loops control scheme. A relevant result of this paper is that, by using the proposed fractional-order D controller, higher phase margin, i.e. higher damping, than with a PD controller is guaranteed in all circumstances. Robust phase margin in contact tasks has not been proven in the previously mentioned controls neither others that can be found in the scientific literature. Flexible link robots are relatively fast systems that require efficient real-time implementations of their controls. Several software packages are available for analysis, design, simulation

and implementation of fractional-order controllers (see [30]).

The remainder of this paper is organized as follows. Section 2 describes the dynamics of a single link flexible robot in the cases of free and constrained motion. Section 3 proposes our robust control scheme. Section 4 presents the experimental platform and some experimental results. Section 5 draws some concluding remarks.

2. System Modelling

We address the control of a single link flexible robot moving in a horizontal plane. Owing to the mass distributed through the link, the dynamics of this robot is described by the Euler-Bernoulli partial differential equation (PDE) of a beam, e.g. [31],

$$EI\frac{\partial^4 w(x,t)}{\partial x^4}+\rho\frac{\partial^2 w(x,t)}{\partial t^2}+\upsilon_l\frac{\partial w(x,t)}{\partial t}=f(x,t) \tag{2}$$

where $f(x,t)$ is a distributed external force and $w(x,t)$ is the elastic deflection measured from the undeformed beam. Moreover, a flexible beam with uniform linear mass density ρ, uniform bending stiffness EI, and a constant damping coefficient υ_l is assumed. Dynamics described by this PDE has infinite vibration modes, i.e., it has transfer functions of infinite order. However, since the amplitude of the vibration modes decreases as their frequency increases, as much as four vibration modes are usually taken into account. The special case of a beam with a mass significantly lower than the mass of its payload has some specific features: 1) only one vibration mode (in the case of a payload with mass and without rotational inertia) or two vibration modes (payload with both mass and rotational inertia) are apparent, and 2) the dynamic model is simpler yielding transfer functions of second, fourth or sixth order (see e.g. [32]).

The following assumptions about our flexible link robot are made in this article:

a) Uniform link section I and elasticity coefficient E through the link.

b) A link of negligible mass, length l, and rotational stiffness coefficient $c=3EI/l$, which is rotated by a motor in a horizontal plane and is not affected by gravity.

c) A payload mass of value of m is concentrated at the tip (in our experimental setup, the mass of the payload is several times the mass of the link).

d) No rotational inertia of the payload at the tip.

2.1. Motor dynamics

The dynamic model of the motor with a reduction gear of ratio $1:n$ is

$$\hat{\Gamma}(t) = \hat{K}_m v(t) = \hat{J}\ddot{\hat{\theta}}_m(t) + \hat{\eta}\,\dot{\hat{\theta}}_m(t) + \hat{\Gamma}_{Coul}(t) + \hat{\Gamma}_c(t) \tag{3}$$

where $v(t)$ is the voltage supplied to the servo-amplifier and $\hat{\theta}_m(t)$ is the motor angle. As it is assumed that the motor is endowed with a servo-amplifier of very fast dynamics, the current of the motor and, then, the motor torque $\hat{\Gamma}(t)$, are assumed to be proportional to the previous control signal $v(t)$. $\hat{K}_m$ is the motor constant that defines such proportionality, $\hat{\eta}$ is the motor viscous friction coefficient, and $\hat{J}$ is the motor rotational inertia. $\hat{\Gamma}_c(t)$ is the coupling torque between the motor and the link seen from the motor side of the gear. $\hat{\Gamma}_{Coul}(t)$ is the Coulomb friction term which is non-linear. Variables and parameters with upper hat are referred to the motor side of the gear. The same variables and parameters without the upper hat are referred to the link side of the gear. For example, the conversion between angles of the motor is $\hat{\theta}_m(t) = n\theta_m(t)$, and the conversion between torques is $\hat{\Gamma}(t) = \Gamma(t)/n$.

2.2. Link dynamics

Consider assumptions a) to d). Assumption b) implies that $\rho = 0$ in (2). Consider that only the tip mass touches the surface of a stationary object and, hence, a force F_l appears on the contact point, exerted by the environment on the link tip, as shown in Fig. 1. Then no forces are exerted at intermediate points of the link and it is therefore verified that $f(x,t) = 0$ in (2). Moreover, assume that the link has no internal distributed damping caused by elasticity. Then $\upsilon_l = 0$. Consequently, equation (2) becomes

$$EI\frac{\partial^4 w(x,t)}{\partial x^4} = 0 \tag{4}$$

whose solution is a deflection function $w(x)$ that is a third order polynomial in x and its coefficients depend on t. Taking this into account together with the boundary conditions at the two ends of the link, the dynamic model of multiple lumped-masses flexible

robots is obtained, see e.g. [33]. Our robot is the simplest case: it has a single lumped mass at the tip. Then its dynamics can be easily obtained from simple well-known mechanical equations as follows.

From the balance of moments with respect to the rotatory axis, the following model is defined for the link dynamics:

$$ml^2 \frac{d^2\theta_l(t)}{dt^2} + \upsilon_0 l^2 \frac{d\theta_l(t)}{dt} = \Gamma_c(t) + lF_l(t) \tag{5}$$

where θ_l is the angle of the tip of the link (and the angle of the payload) and υ_0 is the damping coefficient of the link. The damping term of (5) is different from the distributed damping term presented in (2). This damping depends only on the tip velocity, and experiments have shown that it often provides a good approximation of the overall damping of the link. In this expression, $\Gamma_c(t)$ represents the coupling torque between the motor and the link.

Moreover, from modeling the deflection of the bar under assumptions a) and b), and taking into account the deflection model yielded by (4), the coupling torque $\Gamma_c(t)$ can be expressed as [33]:

$$\Gamma_c(t) = c(\theta_m(t) - \theta_l(t)) \tag{6}$$

Substituting (6) in expression (5) and rearranging terms yields the link dynamics model

$$\frac{d^2\theta_l(t)}{dt^2} + \frac{\upsilon_0}{m}\frac{d\theta_l(t)}{dt} + \frac{c}{ml^2}\theta_l(t) = \frac{c}{ml^2}\left(\theta_m(t) + \frac{l}{c}F_l(t)\right) \tag{7}$$

which has one output θ_l and two inputs θ_m and F_l. Taking Laplace transforms in there and equating the output yields

$$\Theta_l(s) = \frac{\omega_0^2}{s^2 + \frac{\upsilon_0}{m}s + \omega_0^2}\left(\Theta_m(s) + \frac{l}{c}F_l(s)\right) \tag{8}$$

where $\omega_0 = \sqrt{c/(ml^2)}$.

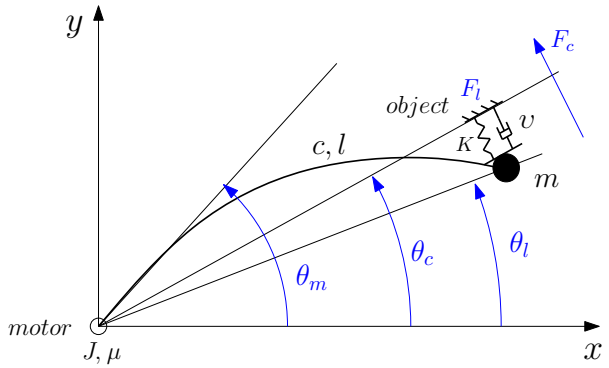

Figure 1: Flexible link actuated by a motor in constrained motion

2.2.1. *Free motion*

In the case that the robot moves freely, link dynamics can be obtained from equation (7) or (8) by just making $F_l = 0$. Then (8) becomes

$$\frac{\Theta_l(s)}{\Theta_m(s)} = \frac{\omega_0^2}{s^2 + \frac{\upsilon_0}{m}s + \omega_0^2} \tag{9}$$

Moreover, taking Laplace transforms in (6) and substituting (9) in there, the following transfer function is obtained:

$$\frac{\Gamma_c(s)}{\Theta_m(s)} = c\frac{s^2 + \frac{\upsilon_0}{m}s}{s^2 + \frac{\upsilon_0}{m}s + \omega_0^2} \tag{10}$$

2.2.2. *Constrained motion*

Assume that, in the constrained motion, the robot-environment contact is produced at the link tip and the environment presents a mechanical impedance given by the well known spring-damper model:

$$F_l(t) = K(y_c - y_l(t)) + \upsilon\frac{d(y_c - y_l(t))}{dt} \tag{11}$$

where K and υ are the stiffness and damping characteristics of the environment, $y_l = l\theta_l$ is the tip position and $y_c = l\theta_c$ is the position of the obstacle, being θ_c the angular position of the impacted surface at the moment of the collision (which is the equilibrium

position at which the obstacle is not compressed neither stretched). This can be expressed in terms of angular displacements as

$$F_l(t) = Kl(\theta_c - \theta_l(t)) + \upsilon l\left(\frac{d\theta_c}{dt} - \frac{d\theta_l(t)}{dt}\right) \tag{12}$$

Due to the fact that y_c is a fixed point and $d\theta_c/dt = 0$, (12) reduces therefore to

$$F_l(t) = Kl(\theta_c - \theta_l(t)) - \upsilon l\frac{d\theta_l(t)}{dt} \tag{13}$$

Substituting (13) in (5) and operating yields

$$ml^2\frac{d^2\theta_l(t)}{dt^2} + (\upsilon_0 + \upsilon)l^2\frac{d\theta_l(t)}{dt} + Kl^2(\theta_l(t) - \theta_c) = \Gamma_c(t) \tag{14}$$

Defining $\triangle\theta_l(t) = \theta_l(t) - \theta_c$ and taking into account that $\ddot{\theta}_c = \dot{\theta}_c = 0$, (14) becomes

$$\Gamma_c(t) = ml^2\frac{d^2}{dt^2}(\triangle\theta_l(t)) + (\upsilon_0 + \upsilon)l^2\frac{d}{dt}(\triangle\theta_l(t)) + Kl^2\triangle\theta_l(t) \tag{15}$$

On the other hand, (6) can be expressed as

$$\Gamma_c(t) = c(\theta_m(t) - \theta_c - \theta_l(t) + \theta_c) = c(\triangle\theta_m(t) - \triangle\theta_l(t)) \tag{16}$$

being $\triangle\theta_m(t) = \theta_m(t) - \theta_c$. Moreover, equation (13) can be expressed as

$$F_l(t) = -Kl\triangle\theta_l(t) - \upsilon l\frac{d}{dt}(\triangle\theta_l(t)) \tag{17}$$

Applying Laplace transforms to (15)–(17), it is obtained:

$$\Gamma_c(s) = \left(ml^2s^2 + (\upsilon_0 + \upsilon)l^2s + Kl^2\right)\triangle\Theta_l(s) \tag{18}$$

$$\Gamma_c(s) = c\left(\triangle\Theta_m(s) - \triangle\Theta_l(s)\right) \tag{19}$$

$$F_l(s) = -\left(Kl + \upsilon ls\right)\triangle\Theta_l(s) \tag{20}$$

The combination of (18) and (19) yields:

$$\frac{\triangle\Theta_l(s)}{\triangle\Theta_m(s)} = \frac{\omega_0^2}{s^2 + \frac{\upsilon_0+\upsilon}{m}s + \left(\omega_0^2 + \frac{K}{m}\right)} \tag{21}$$

and substituting (21) in (19) and (20), the following transfer functions are also obtained:

$$\frac{\Gamma_c(s)}{\triangle\Theta_m(s)} = \frac{c\left(s^2 + \frac{\upsilon_0+\upsilon}{m}s + \frac{K}{m}\right)}{s^2 + \frac{\upsilon_0+\upsilon}{m}s + \left(\omega_0^2 + \frac{K}{m}\right)} \tag{22}$$

$$\frac{F_c(s)}{\triangle\Theta_m(s)} = \frac{l\omega_0^2\left(K + \upsilon s\right)}{s^2 + \frac{\upsilon_0+\upsilon}{m}s + \left(\omega_0^2 + \frac{K}{m}\right)} \tag{23}$$

where $F_c(t)$ is the force exerted by the link on the environment which, as consequence of the Newton's Third Law, is $F_c(t) = -F_l(t)$.

The free motion dynamics can be obtained from (21) and (22) by making $K = \upsilon = 0$ and changing incremental by absolute angles. Transfer functions (21) and (22) will thereafter be used to describe all the cases. They will be denoted as $G_p(s, K, \upsilon)$ and $G_\Gamma(s, K, \upsilon)$ respectively, and the free motion case will be described by these transfer functions making $K = \upsilon = 0$.

Fig. 2 includes a block diagram representation of the link dynamics in both free and constrained motion cases. They are expressed by the interconnection of equations (6), (8) and (20).

3. Control System

This section develops a new fractional-order robust control system for single link flexible robots. It aims to control the tip position in the free motion case and the force exerted by the tip on the environment in the constrained motion case. In order to achieve this, the entire control problem is divided into three parts: 1) free motion control; 2) constrained motion control; and 3) contact detection algorithm.

A unique closed-loop controller is used all the time in order to provide with more robustness to the whole system. Switching between reference trajectories instead of between controllers is carried out when the first contact is detected, as it was done

in [2]. The controller must therefore perform adequately in both free and constrained motion cases, and must be robustly asymptotically stable to:

1. Changes in working operation: from free to constrained motion and vice versa.
2. Rebounds.
3. Unknown mechanical impedance of the environment.
4. Unknown Coulomb friction in the motor of the robot.

The proposed control system must also exert a force on the environment with nearly zero steady state error. Moreover, this controller must yield relatively high values of the phase margin, i.e. relatively high damping, in all the cases. This feature has never been achieved by any of the hybrid position-force control systems already existing for either rigid or flexible link robots.

The contact detection algorithm triggers changes in the reference and the feedforward term of the control system the first time that the robot environment changes, i.e., the first time that the robot changes from free to constrained motion. This algorithm remains inactive during the subsequent state transitions caused by rebounds.

In the proposed control system:

1. The measured variables are $\Gamma_c(t)$ and $\theta_m(t)$.
2. The input of the system is $\triangle\theta_m(t) = \theta_m(t) - \theta_c$. The variable that can be controlled is the motor angle, $\theta_m(t)$. However, θ_c is unknown a priori since it is the angle at which the contact occurs. Therefore, such variable has to be estimated during the contact process in order to adapt the controller, or a controller has to be designed insensitive to that variable.
3. The output variable that is fed back in the closed-loop control system is $\theta_l(t)$ in both the free and constrained motion cases. However, an additional open-loop control is implemented in the constrained motion in order to achieve the desired force value F_c or, equivalently, a desired Γ_c (note that $F_c = \Gamma_c/l$).

In order to fulfill the fourth robustness specification (unknown Coulomb friction), a nested double control loop scheme is proposed. The inner-loop is closed with high gains around the motor. It feeds back the motor position and removes the effects of

the nonlinear Coulomb friction of the motor as well as the effects of time varying viscous friction. The outer-loop is devoted to remove link vibrations. This scheme has demonstrated to be very stable and effective in removing motor friction effects in flexible link robots (e,g. [2], [18], [25], [33]).

The methodology to design the control system is as follows:

1. Design the inner-loop control system in order to remove the friction effects and achieve a motor closed-loop response as fast as possible without saturating the actuator. Standard integer-order controllers have shown to be quite effective in attaining this. Then no further improvements are needed in this control loop and a fractional-order controller is not proposed here. The control structure proposed in [34] is used, which includes a feedback of the coupling torque that makes the dynamics of the controlled motor be insensitive to mechanical changes in the link (including changes in the operating mode: free or constrained motion). This feedback of the coupling torque drastically simplifies the motor dynamic model that is used to design the motor controller, making such design relatively simple.
2. Subsequently, design the outer-loop control in order to robustly damp the link vibrations and carry out the force control. Since robustness concerns 1) to 3) have to be fulfilled and a high phase margin is desired in all cases, a fractional-order controller is designed for this loop.
3. The contact detection mechanism proposed in [2] for a robot similar to the one considered here is implemented.

Figure 2 shows the scheme of the proposed control system, in which $C_1(s)$ and $C_2(s)$ are the controllers of the inner-loop, and $C(s)$ is the fractional-order controller of the outer-loop. The tip angular position, which is fed back in the closed-loop control, is estimated from the measured variables by equating expression (6):

$$\theta_l(t) = \theta_m(t) - \frac{1}{c}\Gamma_c(t) \tag{24}$$

This control scheme is subsequently detailed.

3.1. Motor inner-loop

PID controllers with a low pass filter term ensure good trajectory tracking, compensate disturbances such as unmodeled components of the friction, and are robust to parameter uncertainties, providing precise and fast motor positioning responses. An algebraic methodology is used to tune the parameters of these controllers.

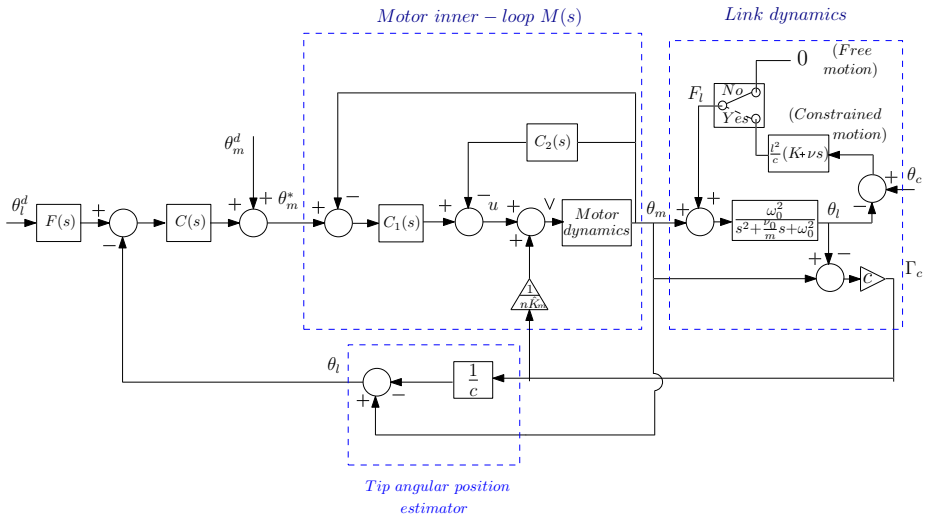

Figure 2: Control scheme of a single-link flexible arm. $\theta_m^d(t)$ and $\theta_l^d(t)$ are the desired motor and tip angular trajectories, respectively. $C(s)$ is the fractional-order controller robust against changes in the mechanical impedance of the contacted object, and $C_1(s)$ and $C_2(s)$ are the *PID* controllers with low-pass filters for the motor inner-loop

The *PID* controller is combined with a feedback term of the coupling torque $\Gamma_c(t)$. Its rationale is the following. Consider the motor dynamics given by (3). If this feedback term is implemented, the input to the motor becomes

$$v(t) = u(t) + \frac{\Gamma_c(t)}{n\hat{K}_m} \tag{25}$$

where $u(t)$ is the control signal provided by the combination of controllers $C_1(s)$ and $C_2(s)$ (see Figure 2) and, substituting this in (3), the motor dynamics reduce to

$$\hat{K}_m u(t) = \hat{J}\ddot{\hat{\theta}}_m(t) + \hat{\eta}\dot{\hat{\theta}}_m(t) + \hat{\Gamma}_{Coul}(t) \tag{26}$$

Moreover, if the Coulomb friction is regarded as a step like disturbance that can be

compensated by the loop closed around the motor, the transfer function from the fictitious input, $u(s)$, to the motor angular position, $\hat{\theta}_m(s)$, can be obtained:

$$\frac{\hat{\theta}_m(s)}{u(s)} = \hat{G}_m(s) = \frac{\hat{K}_m}{s \cdot (\hat{J} \cdot s + \hat{\eta})} \tag{27}$$

The transfer function $G_m(s)$ between the motor angle at the link side of the gear, $\theta_m(t)$, and the fictitious control signal, $u(t)$, is given by $G_m(s) = \hat{G}_m(s)/n$. The proposed *PID* controller is shown in Figure 3 and is defined as:

$$n_1(s) = a_2 s^2 + a_1 s + a_0; \quad n_2(s) = b_2 s^2 + b_1 s + b_0; \quad d(s) = s(s+h) \tag{28}$$

The four closed-loop poles of this system can be arbitrarily placed following the algebraic method described in [35], where all the closed-loop poles were placed in the same location p. Two zeros of the closed-loop are placed in p in order to cancel two poles of the closed-loop. Then the closed-loop transfer function that results for the motor is:

$$M(s) = \frac{\theta_m(s)}{\theta_m^*(s)} = \frac{1}{(1+\varepsilon \cdot s)^2} \; ; \; \varepsilon = -p^{-1} \tag{29}$$

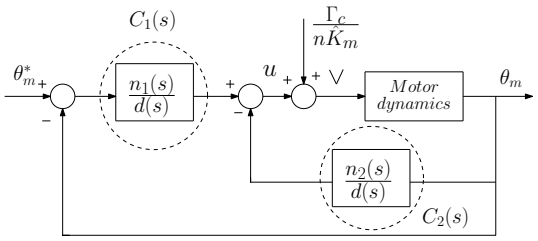

Figure 3: *PID* applied to the motor.

3.2. Trajectory generation

The control system shown in Figure 2 includes a reference for the outer-loop control - which is the desired trajectory of the tip angle $\theta_l^d(t)$ - and a feedforward term - which is the desired trajectory of the motor angle $\theta_m^d(t)$ - that is added to the output of the outer-loop controller $C(s)$. The following lemma proves that the accurate tracking of the desired tip position trajectory $\theta_l^d(t)$ can be achieved by the proposed control

system if reference signals $\theta_l^d(t)$ and $\theta_m^d(t)$ are properly computed by inverting the robot dynamics.

Lemma 1. Let us denote as $\theta_l^d(t)$ the reference trajectory to be tracked by the robot tip position $\theta_l(t)$ in a free motion mode. Assume that the dynamics of the robot under free motion are given by (9), (10) and (29), and that no disturbances neither modeling errors are present. Moreover, consider the control scheme of Fig. 2. If the feedforward term were

$$\theta_m^d(t) = \theta_l^d(t) + \frac{\upsilon_0}{m\omega_0^2}\dot{\theta}_l^d(t) + \frac{1}{\omega_0^2}\ddot{\theta}_l^d(t) \tag{30}$$

and $F(s) = M(s)$, then the tip position would describe a trajectory $\theta_l(t)$ given by

$$\theta_l(t) = m(t) * \theta_l^d(t). \tag{31}$$

where $m(t)$ is the inverse Laplace transform of the $M(s)$ given by (29) and $*$ is the convolution operator.

Proof. The closed-loop transfer functions that relate the output $\theta_l(t)$ with the command signals $\theta_l^d(t)$ and $\theta_m^d(t)$ in the free motion mode are obtained from operating the transfer functions of the scheme of Fig. 2:

$$\Theta_l(s) = M(s)\frac{G_p(s,0,0)\Theta_m^d(s) + C(s)M(s)G_p(s,0,0)\Theta_l^d(s)}{1 + C(s)M(s)G_p(s,0,0)} \tag{32}$$

Taking into account that the Laplace transform of (30) is $\Theta_m^d(s) = G_p^{-1}(s,0,0)\Theta_l^d(s)$, making $F(s) = M(s)$ and simplifying the resulting equation yields that

$$\Theta_l(s) = M(s)\Theta_l^d(s) \tag{33}$$

Taking inverse Laplace transforms in this expression proves the lemma. □

In equation (29), $M(s)$ tends to 1 if $p \to -\infty$ and then, from (33), $\Theta_l(s) \to \Theta_l^d(s)$ and hence $\theta_l(t) \to \theta_l^d(t)$. It is therefore advisable to close the inner-loop with high gain controllers in order to obtain high absolute values of p in $M(s)$ and, then, achieve an accurate tip angle tracking of the reference trajectory $\theta_l^d(t)$.

3.3. Robot outer-loop

It has already been stated that a unique outer-loop controller is used for free and constrained robot motions. Consider a force control scheme in which the process transfer function (22) is used (note that a direct contact force control based on model (23) can not be implemented because the contact force is not measured). It has two lowly damped poles at $p_{1,2} = -\frac{\upsilon_0+\upsilon}{2m} \pm j\sqrt{\frac{K}{m}+\omega_0^2-\left(\frac{\upsilon_0+\upsilon}{2m}\right)^2}$ and two zeros at $z_{1,2} = -\frac{\upsilon_0+\upsilon}{2m} \pm j\sqrt{\frac{K}{m}-\left(\frac{\upsilon_0+\upsilon}{2m}\right)^2}$ in the constrained motion. Since ω_0 has usually a small value, often $K/m >> \omega_0^2$, and poles $p_{1,2}$ are therefore close to zeros $z_{1,2}$. These two poles can therefore be only slightly modified by a closed-loop control. Then this control scheme can hardly add damping to these two poles, which are the dominant ones.

Consider instead closing a control loop of the angular tip position of the robot. This signal could be accurately estimated from (24) if modelling assumptions b) and c) were verified, and the transfer function to be used in the controller design would be (21). This transfer function has no zeros. The poles of the closed-loop system can therefore be easily placed in desired locations, allowing us to move the poles $p_{1,2}$ far away from the imaginary axis, and add damping to the closed-loop system. For this reason Figure 2 presents a scheme that implements a control system of the robot tip angular position instead of the force or torque. The manner in which this control may be used to achieve force control will be described later. Then the link dynamics will thereafter be described by (21) for control purposes.

Due to rebounds, controller $C(s)$ of Figure 2 has to face dynamics that switches between (9) (or (10)) and (21) (or (22)) at unpredictable instants. This controller has therefore to be designed in the framework of the switching (hybrid) systems theory. It is noted that the inner-loop is not affected by this changing dynamics since the motor is connected with the environment only through the link, and the effects of the link on the motor have been compensated by implementing the feedback loop (25).

The design of the robustness issues of the outer-loop control are detailed next.

3.3.1. The Quadratic Stability Condition for our Hybrid System

This article recalls the following result given in [29] on control of fractional-order switching systems, which is an extension of a previous theorem proposed by [36] on

the quadratic stability of stable linear multi-model SISO systems of integer-order.

Consider a multimodel system composed of n fractional-order subsystems, whose transfer functions $H_i(s)$, $1 \leq i \leq n$, switch among them at unpredictable instants. Then this system is quadratically stable (i.e. there exists a Lyapunov function which guarantees the stability) if it were verified that:

1. All the $H_i(s)$ are of the same order.
2. All the $H_i(s)$ are quadratically stable.
3. It is fulfilled that

$$|\arg(H_{ld}(j\omega)) - \arg(H_{kd}(j\omega))| < \frac{\pi}{2}, \qquad \forall \omega, \qquad \forall l,k, \quad 1 \leq l,k \leq n \tag{34}$$

where $H_{ld}(s)$ and $H_{kd}(s)$ are the denominators of $H_l(s)$ and $H_k(s)$, respectively.

In this study, the closed-loop transfer functions H are obtained from the tip angular position transfer functions $G_p(s,K,\upsilon)$, which depend on the contacted object rigidity K and damping υ. A multimodel system $H_i(s)$, $1 \leq i \leq n$, is assumed of n environments defined by n pairs (K_i, υ_i). Moreover, it is considered that $H_1(s)$ is the free movement case, which corresponds to $K_1 = 0$ and $\upsilon_1 = 0$.

This result applied to our robot states that the asymptotic stability of our closed-loop control system robust to rebounds and indeterminate mechanical impedance of the contacted object is guaranteed if the following conditions are simultaneously fulfilled:

1. The closed-loop controlled robot is stable for all the models, which include free motion and tip contacts with any of the considered environments (rigid, elastic...). These environments are characterized by n pairs of values $K_i \geq 0$ and $\upsilon_i \geq 0$. The closed-loop transfer functions are

$$H_i(s) = \frac{C(s)M(s)G_p(s,K_i,\upsilon_i)}{1 + C(s)M(s)G_p(s,K_i,\upsilon_i)}, \qquad 1 \leq i \leq n \tag{35}$$

2. Condition (34) is verified.

Moreover, since $G_p(s,0,0)$ and $G_p(s,K,\upsilon)$ (for any $K,\upsilon > 0$) are of the same order, $H_i(s)$, $1 \leq i \leq n$, are of the same order too, and the result [29] can therefore be applied.

Subsequently, two theorems are proposed that guarantee the fulfillment of the robust quadratic stability condition (34) by a controller $C(s)$ in the case of rebounds. The first theorem deals about the switching condition needed to obtain a stable rebound control between two constrained movements with different contacted objects, i.e., with different mechanical impedances (one of them can be free movement). The other states a sufficient condition to obtain quadratic stable control in the case that the robot switches among a set of objects with different and unknown but bounded stiffness K and damping υ values, i.e., robust switching condition.

In the following, $C_n(s)$ and $C_d(s)$ stand for the numerator and denominator polynomials of $C(s)$, respectively.

Theorem 1. Consider a hybrid system that switches between two linear time invariant systems $H_l(s)$ and $H_k(s)$, belonging to the set (35) of the multimodel system, a finite number of times at unknown instants. Then the fulfillment of the condition

$$|\arg(H_{ld}(j\omega)) - \arg(H_{kd}(j\omega))| < \frac{\pi}{2}, \qquad \forall\omega, \tag{36}$$

where $H_{ld}(s)$ and $H_{kd}(s)$ are the denominator polynomials of $H_l(s)$ and $H_k(s)$ respectively, is equivalent to the fulfillment of the following inequality:

$$\begin{aligned} &\left(X_r(\omega_n) - \omega_n^2 + K'_k\right)\left(X_r(\omega_n) - \omega_n^2 + K'_l\right) + \\ &\left(X_i(\omega_n) + (\upsilon'_0 + \upsilon'_k)\omega_n\right)\left(X_i(\omega_n) + (\upsilon'_0 + \upsilon'_l)\omega_n\right) > 0, \qquad 0 \leq \omega_n < \infty \end{aligned} \tag{37}$$

where ω_n is the normalized frequency $\omega_n = \omega/\omega_0$, $K'_{\{l,k\}} = K_{\{l,k\}}/(m\omega_0^2)$, $\upsilon'_{\{0,l,k\}} = \upsilon_{\{0,l,k\}}/(m\omega_0)$, $X(j\omega_n) = 1 + C(j\omega_n)M(j\omega_n)$, $X_r(\omega_n) = \Re\{X(j\omega_n)\}$ and $X_i(\omega_n) = \Im\{X(j\omega_n)\}$, denoting $\Re$ and $\Im$ the real and imaginary components of X respectively.

Proof. See Appendix A.

Consider the multimodel system case, in which the previous stability condition must be verified when the robot switches among object impedances that belong to a

region defined by the stiffness and damping lower and upper bounds $\left(\underline{K},\overline{K}\right)$ and $(\underline{\upsilon},\overline{\upsilon})$ respectively. In this case, condition (37) must be verified for all the possible combinations of pairs (K_l,υ_l), (K_k,υ_k) that belong to such region. Checking this condition for all the possible cases with a computer is a quite time consuming procedure. The following theorem proposes an equivalent condition that significantly reduces this computation time.

Theorem 2. Consider a hybrid system that switches among a set of linear time invariant systems described by transfer functions $H_i(s)$, given by (35), a finite number of times at unknown instants. Assume that the mechanical impedances of this set of systems are unknown but they belong to a bounded region defined by $\underline{K} \leq K_i \leq \overline{K}$ and $\underline{\upsilon} \leq \upsilon_i \leq \overline{\upsilon}$. Then condition (34) is verified for any switching sequence inside this region if the following condition is fulfilled:

$$\left(X_r(\omega_n)-\omega_n^2+K'_m\right)^2+\left(X_i(\omega_n)+(\upsilon'_0+\upsilon'_m)\omega_n\right)^2>{\delta'_K}^2+\omega_n^2{\delta'_\upsilon}^2,\qquad 0\leq\omega_n<\infty \tag{38}$$

for any pair of values (K'_m,υ'_m) included in the intervals

$$\frac{\underline{K}}{m\omega_0^2}\leq K'_m\leq\frac{\overline{K}}{m\omega_0^2},\quad \frac{\underline{\upsilon}}{m\omega_0}\leq\upsilon'_m\leq\frac{\overline{\upsilon}}{m\omega_0} \tag{39}$$

where the values δ'_K and δ'_υ are given by

$$\delta'_K=min\left(K'_m-\frac{\underline{K}}{m\omega_0^2},\frac{\overline{K}}{m\omega_0^2}-K'_m\right)\geq 0,\quad \delta'_\upsilon=min\left(\upsilon'_m-\frac{\underline{\upsilon}}{m\omega_0},\frac{\overline{\upsilon}}{m\omega_0}-\upsilon'_m\right)\geq 0 \tag{40}$$

ω_n is the normalized frequency $\omega_n=\omega/\omega_0$, $\upsilon'_0=\upsilon_0/(m\omega_0)$, $X(j\omega_n)=1+C(j\omega_n)M(j\omega_n)$, $X_r(\omega_n)=\Re\{X(j\omega_n)\}$, $X_i(\omega_n)=\Im\{X(j\omega_n)\}$.

Proof. See Appendix B.

Remark 1. Note that this theorem reduces the number of times that condition (37) has to be checked - in order to guarantee the switching condition in the region $\left(\underline{K},\overline{K}\right)$ and $(\underline{\upsilon},\overline{\upsilon})$ - from $\frac{1}{2}n^2(n-1)^2$ to $\frac{1}{2}n(n-1)$, being n^2 the number of nodes of the dis-

cretized region, i.e, the region is assumed to be divided in a rectangular grid in which the length of the sides of a cell is $\left(\overline{K}-\underline{K}\right)/(n-1)$ and $(\overline{\upsilon}-\underline{\upsilon})/(n-1)$.

Remark 2. Since the free movement case is included in the multimodel system, the bounds of the impedance region are $\left(0,\overline{K}\right)$ and $(0,\overline{\upsilon})$.

3.3.2. Design of Controllers Robust to an Uncertain Environment

This subsection discusses the structure of the controllers that achieve asymptotic closed-loop stability in the cases $K \geq 0$ and $\upsilon \geq 0$. The design of a controller that verifies the robust phase margin specification is also addressed.

Consider an uncertain environment (K,υ) such that $0 \leq K \leq \bar{K}$ and $0 \leq \upsilon \leq \bar{\upsilon}$, being $\bar{K}$ and $\bar{\upsilon}$ the maximum values for the foreseen contacted objects. A controller has to be designed such that, besides verifying the quadratic stability condition (34):

1. The closed-loop system must be asymptotically stable in the defined range of mechanical impedances, i.e. robust asymptotic stability.
2. The closed-loop system must have a desired dynamic performance in the free movement.
3. The phase margin of the system must be relatively high for any pair (K,υ) that belongs to the defined range of impedances, i.e., robust phase margin condition.

A control system that fulfills these specifications is designed next. Since this article is focused mostly on the contact task, the control scheme of Fig. 2 is considered only in its contact mode. This mode is triggered by the contact detection mechanism and, once it has been set on, it will be never switched off. Switching on this mode only implies changing the reference of the tip angle $\theta_l^d(t)$ (removing prefilter $F(s)$ at certain instant) and the feedforward term $\theta_m^d(t)$ in the manner that will be discussed in a subsequent subsection. Fig. 4 is a simplification of Fig. 2 that will be used thereafter to design the closed-loop controller.

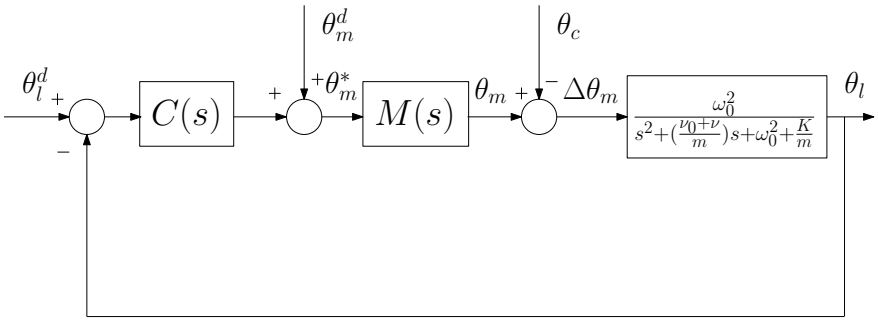

Figure 4: Simplified control scheme of the tip angular position, acting in the contact situation. θ_l^d is the desired (constant) angular tip position, $C(s)$ is the controller robust against changes in the mechanical impedance of the contacted object, and $M(s)$ is represented by its expression (29).

The frequency response of the open-loop system is $L(j\omega) = M(j\omega)G_p(j\omega, K, \upsilon)$. The first path of its Nyquist diagram is represented in Fig. 5. Since a very small value is chosen for the coefficient ε of $M(s)$, usually $M(j\omega) \simeq 1$ at low and medium frequencies, and the open-loop frequency response $L(j\omega)$ can be approximated at these frequencies by $G_p(j\omega, K, \upsilon)$. The first path of this approximate Nyquist diagram is also represented in Fig. 5 in the case of zero damping of the link ($\upsilon_0 = 0$) and the contacted object ($\upsilon = 0$), which is the worst-case scenario for closed-loop stabilization.

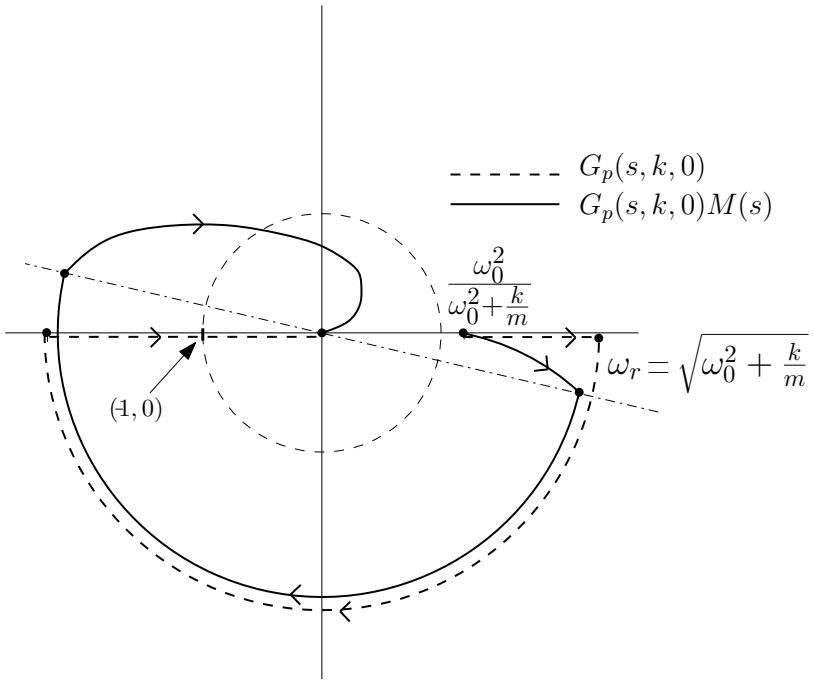

Figure 5: First path of the Nyquist diagram of the robot (with and without including the inner-loop dynamics).

Fig. 5 shows that the approximate system $G_p(j\omega,K,0)$ is marginally stable and the complete system $M(j\omega)G_p(j\omega,K,0)$ would yield an unstable closed-loop system. This figure also shows that the controller $C(j\omega)$ has to add phase to the previous Nyquist plots - at least in the range of frequencies from zero to the gain crossover frequency ω_c - in order to increase the phase margin of the system. Increasing the phase margin produces increasing the relative stability and damping of the system. This suggests that these controllers have to be phase-lead compensators. Moreover, Fig. 5 suggests that, in order to obtain a closed-loop stable system, the gain crossover frequency ω_c must be higher than the resonant frequency ω_r.

We use two specifications to define the closed-loop dynamic performance in the free movement case: damping and settling time. Since these values are related to frequency specifications: damping to phase margin ϕ and settling time to gain crossover frequency ω_c, e.g. [37], the pair $(\phi_0,\ \omega_{c0})$ will be used as control design specifications.

These can be achieved by fulfilling the following complex condition

$$C(j\omega_{c0})M(j\omega_{c0})G_p(j\omega_{c0},0,0) = -e^{j\phi_0} \tag{41}$$

Since two specifications are searched, the simplest phase-lead controllers that can be used must provide two parameters to be tuned. Then two controllers are proposed:

$$C_i(s) = \frac{k_d s + k_p}{(1+\mu s)^2} \tag{42}$$

which is the standard phase-lead controller (a *PD* controller) with parameters k_d and k_p to be tuned, and

$$C_f(s) = \frac{k_f s^\alpha}{(1+\mu s)^2} \tag{43}$$

which is a fractional-order phase-lead controller (a D^α controller) with parameters k_f and α to be tuned. Denominators have been added to the two controllers in order to make them proper and, more important, filter the noise that is present in the feedback signals provided by strain gauge sensors (coupling torque $\Gamma_c(t)$). Parameter μ is chosen small enough so that it only slightly influences the frequency response in the range of frequencies from zero to the gain crossover frequency.

Condition (41) particularized to controller (42) becomes

$$\frac{jk_d\omega_{c0} + k_p}{(1+j\mu\omega_{c0})^2} \frac{\omega_0^2}{(1+j\varepsilon\omega_{c0})^2\left(\omega_0^2 - \omega_{c0}^2 + j\frac{\upsilon_0}{m}\omega_{c0}\right)} = -e^{j\phi_0} \tag{44}$$

which yields, after operating, that

$$jk_d\omega_{c0} + k_p = \chi \tag{45}$$

being

$$\chi = -\frac{e^{j\phi_0}(1+j\mu\omega_{c0})^2(1+j\varepsilon\omega_{c0})^2\left(\omega_0^2 - \omega_{c0}^2 + j\frac{\upsilon_0}{m}\omega_{c0}\right)}{\omega_0^2} \tag{46}$$

a complex number that is calculated from the specifications, the process transfer func-

tion and μ. Denoting χ_r and χ_i as the real and imaginary components of χ respectively, and equating apart the real and imaginary components of (45), the parameters of the *PD* controller are calculated from the expressions

$$k_p = \chi_r, \quad k_d = \chi_i/\omega_{c0} \tag{47}$$

It is easy to check that this closed-loop system can be stabilized only if $k_d > 0$. This implies that the phase of χ must be between 0 and 180 degrees. Imposing this condition on (46) gives an inequality that must be fulfilled by the specifications in order to yield a stable system:

$$0 < \phi_0 + 2arctan(\mu\omega_{c0}) + 2arctan(\varepsilon\omega_{c0}) - arctan\left(\frac{\frac{\upsilon_0}{m}}{\omega_{c0}^2 - \omega_0^2}\right) < \pi \tag{48}$$

in which it has been assumed that $\omega_{c0} > \omega_0$. Since it must be verified that $\omega_{c0} > \omega_r = \sqrt{\omega_0^2 - \left(\frac{\upsilon_0}{2m}\right)^2}$ and υ_0 is usually very small, we have that $\omega_0 \simeq \omega_r$ and the above assumption is suitable.

Condition (41) particularized to controller (43) becomes

$$\frac{k_f(j\omega_{c0})^\alpha}{(1+j\mu\omega_{c0})^2}\frac{\omega_0^2}{(1+j\varepsilon\omega_{c0})^2\left(\omega_0^2 - \omega_{c0}^2 + j\frac{\upsilon_0}{m}\omega_{c0}\right)} = -e^{j\phi_0} \tag{49}$$

which yields, after operating, that

$$k_f(j\omega_{c0})^\alpha = k_f e^{j\frac{\pi}{2}\alpha}\omega_{c0}^\alpha = \chi \tag{50}$$

being χ given also by (46). Denoting $|\chi|$ and $\angle\chi$ as the magnitude and phase of χ respectively, and equating apart the magnitudes and phases of (50), the parameters of the D^α controller are calculated from the expressions

$$\alpha = \frac{2}{\pi}\angle\chi, \quad k_f = |\chi|/\omega_{c0}^\alpha \tag{51}$$

It is easy to check that this closed-loop system can be stabilized only if $0 < \alpha < 2$ and $k_f > 0$. This last condition is always verified as it is apparent from (51). Besides,

the condition on α implies that the phase of χ must be between 0 and 180 degrees which is verified if inequality (48) is fulfilled.

Assume that controllers $C_i(s)$ and $C_f(s)$ have the same value μ and are designed to fulfill the same pair of specifications $(\phi_0,\ \omega_{c0})$. Then both controllers are designed using the same χ value. Equating (45) and (50) yields that

$$jk_d\omega_{c0}+k_p=k_f(j\omega_{c0})^\alpha=jk_fsin\left(\frac{\pi}{2}\alpha\right)\omega_{c0}^\alpha+k_fcos\left(\frac{\pi}{2}\alpha\right)\omega_{c0}^\alpha \tag{52}$$

Equating apart the real and imaginary components of this equation yields

$$k_p=k_fcos\left(\frac{\pi}{2}\alpha\right)\omega_{c0}^\alpha,\qquad k_d=k_fsin\left(\frac{\pi}{2}\alpha\right)\omega_{c0}^{\alpha-1} \tag{53}$$

These expressions show that if $\alpha>1$ in $C_f(s)$, then $k_p<0$ in $C_i(s)$, and vice versa.

Theorem 3. Consider the linear time invariant system $G_p(s,0,0)M(s)$ that describes the free movement case, given by (21) and (29). Let a control system be implemented by either using controller $C_i(s)$ given by (42) or controller $C_f(s)$ given by (43). Assume that both controllers are designed to attain the same frequency specifications (ϕ_0,ω_{c0}) using the same μ value. Then the region of specification points (ϕ_0,ω_{c0}) that can be attained using controllers $C_f(s)$ is larger than using controllers $C_i(s)$ because, besides the common condition (48), $C_i(s)$ must verify an additional condition:

$$k_p>-1 \tag{54}$$

Proof. See Appendix C.

This theorem states that, given a pair of specifications (ϕ_0,ω_{c0}) that verify (48), a controller $C_f(s)$ - with parameters k_f, α - can be always found. In the case that $\alpha<1$, the equivalent $C_i(s)$ controller (the one that verifies these specifications) also exists. However, in the case that $\alpha>1$, the equivalent controller $C_i(s)$ only exists if it were verified that

$$k_f\omega_{c0}^\alpha<-\frac{1}{cos\left(\frac{\pi}{2}\alpha\right)} \tag{55}$$

This inequality is easily obtained from substituting the first equation of (53) in (54).

Subsequently, the robustness of the integer and fractional-order controllers to changes in the parameters of the robot-environment system is analyzed. In many works, only stability robustness is assessed. This study goes beyond in the sense that it seeks to assess, besides stability robustness, phase margin robustness of the closed-loop system. Parameter μ is thereafter made zero since it should be chosen such that the denominators of $C_i(s)$ and $C_f(s)$ influence minimally the frequency response of the open-loop system in the range of frequencies of interest. This simplification facilitates the subsequent calculations.

First, two lemmas about the stability of the considered controllers in the case of contact with stiff objects are presented.

Lemma 2. Consider the linear time invariant system $G_p(s,K,\upsilon)M(s)$ given by (21) and (29), and that a control system is implemented using a controller $C_i(s)$ given by (42) in which $\mu = 0$. Assume an environment without damping, i.e., $\upsilon = 0$. Assume too that $\upsilon_0 = 0$ since the damping of the robot link is usually very small. Then the necessary and sufficient conditions required to stabilize such closed-loop system are

$$k_d < \frac{2}{\varepsilon\omega_0^2} \tag{56}$$

$$\frac{k_d}{2\varepsilon}\left(1-0.5\varepsilon\omega_0^2 k_d-\varepsilon^2\left(\frac{K}{m}+\omega_0^2\right)\right) > k_p > -\frac{K}{m\omega_0^2}-1 \tag{57}$$

Consequently, the gain k_p would be negative in the case of values of K that verify

$$K > m\left(\frac{1-0.5\varepsilon\omega_0^2 k_d}{\varepsilon^2}-\omega_0^2\right) \tag{58}$$

Proof. The characteristic equation of the closed-loop system assuming zero damping ($\upsilon = \upsilon_0 = 0$) is

$$\left(s^2+\frac{K}{m}+\omega_0^2\right)(1+\varepsilon s)^2+\omega_0^2\left(k_d s+k_p\right)=0 \tag{59}$$

The stability conditions yielded by the Routh table are:

$$\begin{aligned} 1-0.5\varepsilon\omega_0^2 k_d &> 0 \\ k_d\left(1-\varepsilon^2\left(\frac{K}{m}+\omega_0^2\right)-0.5\varepsilon\omega_0^2 k_d\right)-2\varepsilon k_p &> 0 \\ \frac{K}{m}+\omega_0^2+\omega_0^2 k_p &> 0 \end{aligned} \tag{60}$$

The first two conditions are the inequalities stated in the lemma and the third condition is always verified. □

Lemma 3. Consider the linear time invariant system $G_p(s,K,\upsilon)M(s)$ given by (21) and (29), and that a control system is implemented using a controller $C_f(s)$ given by (43) in which $\mu = 0$. Assume an environment without damping, i.e., $\upsilon = 0$. Assume also that $\upsilon_0 = 0$. Then a necessary condition to stabilize such closed-loop system is, provided that $k_f > 0$, that

$$\alpha > \frac{4}{\pi} arctan\left(\varepsilon\sqrt{\omega_0^2+\frac{K}{m}}\right) \tag{61}$$

Moreover, the fractional order α would be higher than 1 if it were verified that

$$K > m\left(\frac{1}{\varepsilon^2}-\omega_0^2\right) \tag{62}$$

Proof. The frequency response of the closed-loop system assuming zero damping ($\upsilon = \upsilon_0 = 0$) is

$$G_p(j\omega,K,0)M(j\omega)C_f(j\omega) = \frac{\omega_0^2 k_f (j\omega)^\alpha}{(1+j\varepsilon\omega)^2\left(\omega_0^2+\frac{K}{m}-\omega^2\right)} \tag{63}$$

Since the gain crossover frequency ω_c must be higher than the resonant frequency $\omega_r = \sqrt{\frac{K}{m}+\omega_0^2}$, the phase at this frequency would be $\frac{\pi}{2}\alpha - 2arctan(\varepsilon\omega_c) - \pi$ and the phase margin would be $\phi = \frac{\pi}{2}\alpha - 2arctan(\varepsilon\omega_c)$. Taking into account that $arctan(\varepsilon\omega_c) > arctan(\varepsilon\omega_r)$, it is obtained that $\phi < \frac{\pi}{2}\alpha - 2arctan(\varepsilon\omega_r)$. Closed-loop stability implies a positive phase margin which forces the right side of the previous inequality to be positive. This yields condition (61). Condition (62) easily follows from (61). □

The previous lemmas show that, in order to obtain robust stability when the contact is produced with stiff objects (high values of K), the PD controller needs a negative gain k_p and the D^α controller needs a value $\alpha > 1$. The two following lemmas are devoted to demonstrate that, in these two cases, adding damping to the object increases the phase margin.

Lemma 4. Consider the linear time invariant system $G_p(s,K,\upsilon)M(s)$ given by (21) and (29), and that a control system is implemented using a controller $C_i(s)$ given by (42). Assume an environment without damping, i.e., $\upsilon = 0$. Assume also that $\upsilon_0 = 0$. Then adding damping to the mechanical impedance of the contacted object, i.e., making $\upsilon_0 + \upsilon > 0$, produces a decrease of the gain crossover frequency and, in the case that $k_p < 0$, an increase of the phase margin of $G_p(j\omega,K,\upsilon)M(j\omega)C_i(j\omega)$.

Proof. See Appendix D.

Lemma 5. Consider the linear time invariant system $G_p(s,K,\upsilon)M(s)$ given by (21) and (29), and that a control system is implemented using a controller $C_f(s)$ given by (43). Assume an environment without damping, i.e., $\upsilon = 0$. Assume also that $\upsilon_0 = 0$. Then adding damping to the mechanical impedance of the contacted object, i.e., making $\upsilon_0 + \upsilon > 0$, produces a decrease of the gain crossover frequency and an increase of the phase margin of $G_p(j\omega,K,\upsilon)M(j\omega)C_f(j\omega)$ if $k_f > 0$ and $\alpha < 2$.

Proof. See Appendix E.

Subsequently, two theorems are provided that compare the phase margin robustness of controllers $C_i(s)$ and $C_f(s)$ in the case of a system without damping in the confidence that, according to lemmas 4 and 5, adding damping increases the phase margin in both cases.

Theorem 4. Consider the linear time invariant system $G_p(s,K,\upsilon)M(s)$ given by (21) and (29), and that a control system may be implemented using either a controller $C_i(s)$ given by (42) or a controller $C_f(s)$ given by (43), in both cases with $\mu = 0$. Assume: 1) an environment without damping, i.e., $\upsilon = 0$, 2) no damping in the link, i.e., $\upsilon_0 = 0$ and 3) the motor dynamics of the inner loop can be made very fast so that $\varepsilon = 0$ (and then $M(s) = 1$). Moreover, assume that both controllers are designed for the nominal plant which is the free movement case, i.e., $K = 0$, using the same frequency specifications (ϕ_0, ω_{c0}). Then the robustness of both control systems (with respect to

the nominal plant) to changes in the stiffness K verify that:

- If $\alpha < 1$ or, equivalently, $k_p > 0$: 1) controller $C_i(s)$ yields higher gain crossover frequencies than $C_f(s)$, and 2) $C_i(s)$ yields higher phase margins than $C_f(s)$, for any stiffness value $K > 0$.

- If $\alpha > 1$ or, equivalently, $k_p < 0$: 1) controller $C_f(s)$ yields higher gain frequencies than $C_i(s)$, and 2) $C_f(s)$ yields higher phase margins than $C_i(s)$, for any stiffness value $K > 0$.

Proof. See Appendix F.

According to Lemmas 2 and 3, stable contact with stiff objects is obtained only using integer order controllers $C_i(s)$ having $k_p < 0$ or fractional-order controllers $C_f(s)$ having $\alpha > 1$, respectively. Moreover, Theorem 4 has shown that $C_f(s)$ provides more phase margin and a higher gain crossover frequency to the system for any stiffness value K than $C_i(s)$ if $\alpha > 1$. Then the following theorem, which pursues to generalize the results of Theorem 4 to the case of $\varepsilon > 0$, is focused only on the case that $\alpha > 1$.

Theorem 5. Consider the linear time invariant system $G_p(s, K, \upsilon)$ given by (21), and that a control system may be implemented using either a controller $C_i(s)$ given by (42) with $k_p < 0$, or a controller $C_f(s)$ given by (43) with $\alpha > 1$, in both cases with $\mu = 0$. Assume an environment without damping, i.e., $\upsilon = 0$, and that $\upsilon_0 = 0$. Moreover, assume that both controllers are designed for the nominal plant which is the free movement case, i.e., $K = 0$, using the same frequency specifications (ϕ_0, ω_{c0}). Then the robustness of both control systems with respect to changes in the stiffness K verify that:

1. Controller $C_f(s)$ always yields a higher gain crossover frequency than $C_i(s)$ for any K.
2. Controller $C_f(s)$ yields a higher phase margin than $C_i(s)$ for any K if the following sufficient conditions were simultaneously verified:

$$\kappa \leq \left(1 + \varsigma^2\right) \left(1 - \left(\frac{\omega_0}{\omega_{c0}}\right)^2\right) \tag{64}$$

in which $\varsigma = \varepsilon\omega_{c0}$ and $\kappa = \omega_0^2\omega_{c0}^2 k_f$, and

$$\kappa \leq \begin{pmatrix} \alpha^4 & \alpha^3 & \alpha^2 & \alpha & 1 \end{pmatrix} \Psi \begin{pmatrix} \varsigma^5 \\ \varsigma^4 \\ \varsigma^3 \\ \varsigma^2 \\ \varsigma \\ 1 \end{pmatrix} \tag{65}$$

in the intervals $0 < \varsigma \leq 1$, $0 < \kappa \leq 2$ and $1.05 \leq \alpha \leq 1.95$, where

$$\Psi = \begin{pmatrix} -222.63 & 628.55 & -632.333 & 259.465 & -21.67 & -11.22 \\ 1376.54 & -3885.34 & 3908.39 & -1603 & 132.93 & 69.2 \\ -3192.55 & 9017.28 & -9091.644 & 3743.78 & -322.29 & -158.92 \\ 3291.44 & -9313.29 & 9436.3 & -3921.25 & 366.07 & 160.28 \\ -1273.93 & 3616.9 & -3694.8 & 1561.6 & -165.59 & -58.36 \end{pmatrix} \tag{66}$$

Proof. See Appendix G.

Remark 3. The considered range $0 < \varsigma \leq 1$ is reasonable since the dynamics of the actuator (inner motor loop), which is represented by a cutoff frequency of an approximate value ε^{-1}, should be faster than the response achieved by the controller in the overall system, which may be approximately represented by ω_{c0}. This yields the above upper limit for ς.

Remark 4. Since condition (64) implies that $\kappa \leq 1 + \varsigma^2$, and taking into account the range of ς indicated in Remark 3, the range $0 < \kappa \leq 2$ is justified.

Remark 5. Values of α higher than 2 are inappropriate because noise and the neglected high vibration modes of the robot may be undesirably amplified by the controller. This justifies using fractional orders in the range $1 < \alpha < 2$.

3.4. Contact detection mechanism

The real time contact detection mechanism is described here. The control system of Figure 2 switches its reference θ_l^d and the feedforward term θ_m^d when the robot tip

contacts an object. This mechanism is very simple, and is based on detecting significant differences between the desired coupling torque Γ_c^d (which is the torque that has to be transmitted to the link by the motor in order to follow the desired trajectory, and it is easily calculated from θ_l^d and θ_m^d using expression (6)) and the coupling torque Γ_c measured by the strain gauges. If this difference is noticeable, it means that an external force is being exerted at the tip, and contact happened. The detection algorithm is:

$$|\Gamma_c^d - \Gamma_c| > \gamma \tag{67}$$

where γ is a threshold which depends on the maximum trajectory tracking error allowed during the free motion. This algorithm has been successfully used in [2].

Subsequently, the collision detection mechanism is deactivated and the controller has to achieve the desired contact force with nearly zero steady state error while dealing with rebounds.

3.5. Control of the force exerted by the tip on the environment

In this subsection, a new methodology is proposed to control the force exerted by the robot tip on the environment in the constrained motion case, using the control scheme of Figure 2. The objective is to exert a force F_c^d or, equivalently, a torque $\Gamma_c^d = F_c^d \cdot l$. The idea is to change the references θ_m^d and θ_l^d in different instants, once the impact has been detected, with the objective of controlling the contact force. The advantage of changing the references instead of changing the control scheme or the controller law is that the stability of the system is not affected by environment impedance changes, provided that conditions presented in Section 4 are fulfilled. The methodology has therefore the following stages:

1. The link moves freely using the proposed control scheme until it hits an object.
2. At the instant t_1 at which the collision is detected by the mechanism (67): 1) the control state is changed from the free motion mode to the constrained motion mode, 2) the collision detection mechanism is turned off and 3) the link continues moving trying to follow the commanded trajectory. After the contact has been

established, the coupling torque $\Gamma_c(t)$ keeps increasing as consequence of the motor movement.

3. At the instant t_2 at which $\Gamma_c(t)$ reaches the reference value Γ_c^d: 1) the value of the tip angle reference is changed to $\theta_l^d = \theta_l(t_2)$, 2) prefilter $F(s)$ is removed and 3) the value of the feedforward term is changed to $\theta_m^d = \theta_l^d + \frac{\Gamma_c^d}{c}$. These values are maintained until the coupling torque has reached its steady state. The condition used to determine when such steady state has been reached is

$$\frac{\sigma(\Gamma_c(t))}{|\overline{\Gamma}_c(t)|} < \Lambda \tag{68}$$

being $\sigma(\Gamma_c(t))$ and $\overline{\Gamma}_c(t)$ the standard deviation and the mean values respectively of the coupling torque in a time window $[t-\Delta, t]$ whose length, Δ, is adjusted experimentally. Λ is a threshold that is also experimentally determined. Note that if the steady state motor and tip positions coincided with θ_m^d and θ_l^d respectively, the steady state coupling torque would coincide with Γ_c^d, in accordance with (6), and the force control process would not require any further step.

4. Consider the instant t_3 at which condition (68) is reached. If $\Gamma_c(t) = \Gamma_c^d$, this stage would not be required while if $\Gamma_c(t_3) \neq \Gamma_c^d$, this stage would have to be carried out. Such difference appears because the state of the link is distinct at instant t_2, at which the robot is moving and the coupling torque has components due to the tip mass inertia and the damping of the environment, that at instant t_3, at which the robot is quiet and these components are not present. In the case that such difference is apparent: 1) the reference value is changed to $\theta_l^d = \theta_l(t_3)$ and 2) the value of the feedforward term is changed to $\theta_m^d = \theta_l^d + \frac{\Gamma_c^d}{c}$. These updating laws were obtained under the assumption that the tip position θ_l^d that would yield the desired coupling torque Γ_c^d is approximately $\theta_l(t_3)$. This assumption was made because when the link is in contact with an object in its steady-state, the angle of the motor may be varied producing a significant variation in the coupling torque, whereas the variation of the angle of the tip is very limited by the stiffness of the environment. Notice that if $K \to \infty$, the variation of the angle of the tip would tend to zero when the angle of the motor varies. The

above mentioned moment components caused by the tip mass inertia and the environment damping, that are present in $\Gamma_c(t_2)$, yield a value $\Gamma_c(t_3)$ different of Γ_c^d. This difference is noticeable but, however, small in many cases because accelerations and velocities of the tip in the contact situation are small. Then, since $\Gamma_c(t_3)$ is close to Γ_c^d, small robot changes are required, and the assumption that the tip angle negligibly varies during the stage of fine adjustment of the contact torque is acceptable (however, the motor angle may change significantly in order to attain the desired contact force value).

4. Experimental Setup

4.1. Description of the platform

In this work, a slender antenna made of carbon fiber has been used as lightweight flexible link in order to verify the proposed control scheme. The link is attached to a DC mini servo actuator PMA-5A motor set (from harmonic drive) which includes a reduction gear $n = 100$. The sensory system has an incremental optical encoder to measure the angular position of the motor, θ_m, and a sensor in the base of the link which measures the forces and the torques in the three abscissas (F-T sensor). This sensor is used to measure the coupling torque, Γ^{coup}. Movements are produced only in the horizontal plane. Then gravity effects are not considered in this movement and only the component of the coupling torque in the vertical direction is used. Figure 6 is a photograph of the experimental platform impacting with the object used in this work.

A central processing unit (CPU) is used to implement the controller. All the devices are connected together through the data acquisition (DAQ) driver software NI PCI-6229 Board. The system runs under Microsoft Windows 7, Intel Core (TM) 2 Quad CPU, Q660 2.4 GHz with 3 GB of RAM. The data acquisition and control algorithms are programmed using Labview 10.0. The sampling time of the system data acquisition (control signals, measurements and written data) is $T_s = 0.001$ s. System simulations, identification and comparisons are performed using Simulink/MATLAB R2010a.

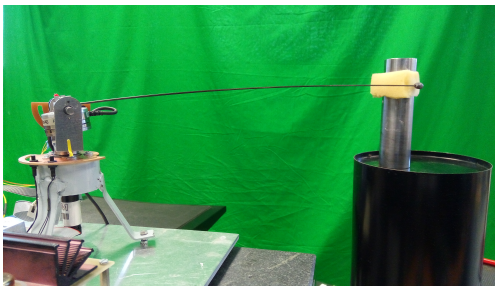

Figure 6: Experimental platform impacting with the object.

The characteristics of the link are shown in Table 1, where its stiffness constant, c, and the vibration frequency, ω_0, were obtained experimentally. ρ is the linear density of the link, l is the length of the link, r is the radius of the circular section of the link and m is the mass at the tip of the link.

Table 1: Flexible-link characteristics.

Feature	Value	Unit
l	0.505	m
r	0.001	m
ρ	$4.7 \cdot 10^{-3}$	kg/m
m	9.98	g
c	0.5686	Nm
ω_0	14.95	rad/s

The assumption b) made in Section 2 of a massless link and that only the tip payload mass has to be considered in the robot dynamics is therefore valid because the mass of the payload ($m_p = 9.98$ g) is several times the weight of the link ($m_l = 2.37$ g).

Table 2 shows the parameters of the motor. V_s and V_{Coul} are the saturation and the Coulomb friction of the motors respectively, in terms of voltage. V_{Coul} is the 33.3 % of the saturation limit V_s. Then, Coulomb friction is very noticeable in our motor.

Table 2: Parameters of the motors.

$\hat{K}(Nm/V)$	$\hat{J}_i(kgm^2)$	$\hat{v}_i(kgm^2/s)$	$V_{Coul}(V)$	$V_s(V)$	n
0.21	6.18×10^{-3}	3.04×10^{-2}	0.4	1.2	100

4.2. *Identification of the flexible link*

The transfer function $G_p(s,0,0)$ has been identified experimentally. The method described in [38] has been employed here because it is easy to use and is well suited to systems with little damping and very decoupled vibration modes. This identification process was performed using a Chirp signal as input, which stimulated the different vibration modes. This signal has an amplitude of 0.02 V and a range of frequencies from 0.01 Hz to 50 Hz in 80 s. Model (9) was then fitted to the frequency response experimentally obtained. In order to obtain the frequency response data of the tip position, the tip position was estimated from motor position and coupling torque measurements using (24). The model approximated to such experimental data is:

$$G_p(s,0,0) = \frac{14.1^2}{s^2 + 0.6s + 14.1^2} \tag{69}$$

The magnitudes of the frequency responses obtained in experimentation and from the approximated model are shown in the upper half of Figure 7 and the phases are shown in the lower half of this figure.

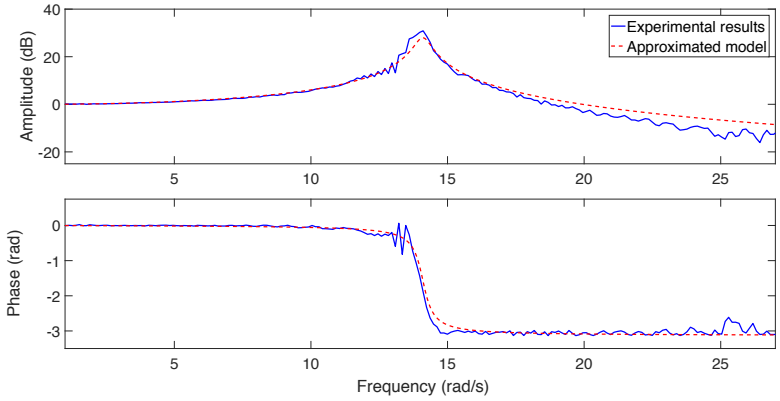

Figure 7: Identification of the flexible link.

Figure 7 shows that:

1. Only one vibration mode is observed (a single resonant peak in the magnitude and a single sharp change of 180° in the phase). Since flexible links with dis-

tributed mass have an infinite number of vibration modes, this experimental result supports the hypothesis of a massless link with all the robot mass concentrated at its tip. Moreover, if a massless flexible link had a mass at its tip that exhibits rotational inertia, the frequency response would had shown two vibration modes. Since only one mode is apparent, the hypothesis of zero rotational inertia at the tip is justified.

2. Model (9) fits very well the experimental data. Then all the hypotheses made in the Modelling section about the mechanical part of our robot are supported by experiments and the assumed values of the mechanical parameters are correct.

4.3. Identification of the environment

A soft and elastic object made of foam was used in this work. The impedance of the object (stiffness and damping characteristics) was identified carrying out two kinds of experiments:

1. The antenna impacts the object using only motor control. The damping is determined by estimating the damping of the coupling torque response from the instant of the impact to the instant at which the response reaches its steady-state.
2. The tip of the link is placed in contact with the object but without exerting any force ($\Gamma_c = 0$). Then the angle of the impacted surface is obtained as $\theta_c = \theta_m$ since in this case the motor position coincides with the tip position and with the contact angle. The control system is used to move the tip of the link into the object. Then a step reference of the tip position is commanded which produces an interaction with the environment measured by the coupling torque. Once the steady state has been reached, equation (14) yields the relationship $Kl^2(\theta_l - \theta_c) = \Gamma_c$. This expression allows to estimate K since Γ_c is measured and θ_l is estimated from (6) and the measurement of θ_m.

Table 3 presents the values of the impedance of the environment for different forces (or coupling torques) exerted to the object. It shows that the damping and stiffness of the object vary with the exerted force. Our control system has therefore to face switching among the different impedances existing in our foam, besides switching with the

free movement dynamics (rebounds case). This justifies the interest of our Subsection 3.3.1 about switching in a multimodel system with more than two models.

Table 3: Object impact characteristics.

n_e	Γ_c	$K(\frac{N}{m})$	$\nu(\frac{N \cdot s}{m})$
1	0.067	6.60	0.16
2	0.076	7.34	0.17
3	0.101	8.48	0.18
4	0.145	9.44	0.19
5	0.161	9.67	0.19
6	0.183	9.91	0.20

4.4. Controller design

Choosing $p = -60$ (the closed-loop poles of the inner-loop), and following the algebraic method of Subsection 3.1, the parameters of the controller (see Figure 3) are given in Table 4.

Table 4: Motor controller parameters (inner-loop)

a_2	a_1	a_0	b_2	b_1	b_0	h
74.16	8899.2	267000	347	8899.2	0	235

A filter $1/(1+0.01s)^2$ was found adequate to remove the high frequency noise present in $\Gamma_c(t)$. Then, it was made $\mu = 0.01$ in controller (43).

The controller of the outer loop was designed to achieve a phase margin $\phi_0 = 60^\circ$ for the nominal system (free movement case). The gain crossover frequency and, therefore, the parameters of the controller (through expressions (46) and (51)), were tuned choosing a value of ω_{c0} such that: 1) $\omega_{c0} > \omega_0$, 2) the closed-loop system remains stable for all the impedances presented in Table 3, 3) the quadratic stability condition is verified for our multimodel system that includes the free movement model and all the models of the robot-environment interaction defined by Table 3 and 4) fractional order α is as low as possible in order to prevent amplification of the sensor noise. Lemmas 2 and 4 helped to check condition 2) and Theorem 2 was used to assess the quadratic stability condition 3). The gain crossover frequency obtained after this design process

is $\omega_{c0} = 30$ rad/s and the controller yielded by the pair of frequency specifications is:

$$C(s) = 0.018\frac{s^{1.6}}{(1+0.01s)^2} \tag{70}$$

Note that the condition of Theorem 3 is not verified (it can be checked that inequality (55) is not fulfilled). Then a *PD* controller equivalent to the designed D^{α} controller does not exist for the pair of chosen nominal specifications.

Figure 8 shows the region where the system (69) under interaction with the environment and controlled by (70) is quadratically stable for different values of K and ν. The values of the impedances of Table 3 and the zero impedance case (which corresponds to the free movement) are also depicted. This figure shows that all these cases are included in this region.

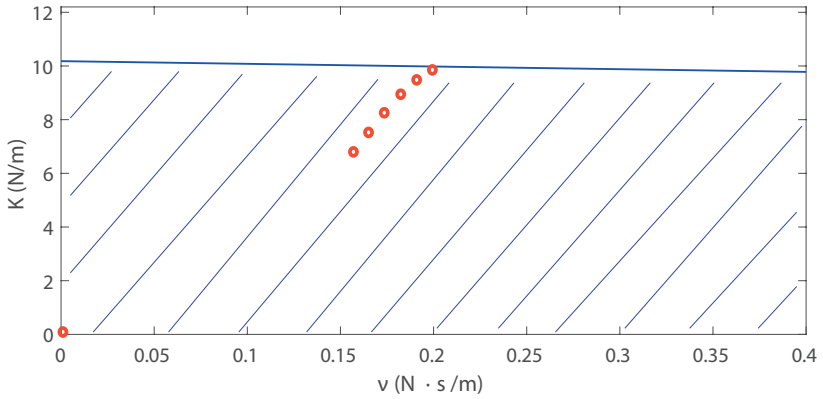

Figure 8: Quadratically stable region.

The difference of phases existing between the characteristic polynomials of the free and constrained motion closed-loop systems is illustrated in Fig. 9 for three representative impedances among the ones presented in Table 3: a) $K = 6.60$, $\nu = 0.16$, b) $K = 8.48$, $\nu = 0.18$ and c) $K = 9.91$, $\nu = 0.2$. It can be seen that specification (34) is fulfilled and, then, rebounds between free and constrained motion are avoided.

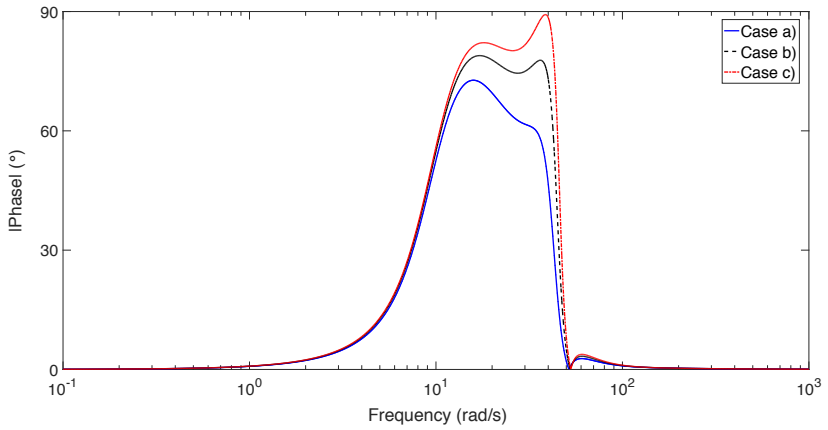

Figure 9: Absolute value of the phase difference between the free and constrained motion characteristic polynomials of the closed-loop system when impacting objects having different stiffness and damping

Figure 10 shows the Bode diagrams of the open-loop system in the cases of the free motion and the three constrained motions previously mentioned. Note the low magnitude at low frequencies caused by the fractional derivative of the numerator of the controller.

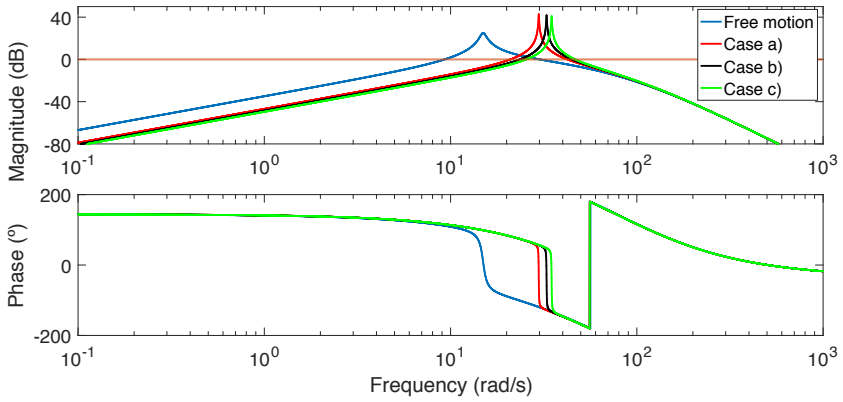

Figure 10: Bode diagrams of the open-loop system $C(s)M(s)G_p(s,K,\upsilon)$ in the cases of free motion and constrained motion with the three mentioned impedances

Figure 11 shows the Bode diagrams of the control system of Figure 2 in the cases of the free motion and the three constrained motions previously mentioned. The repre-

sented closed-loop transfer functions are

$$\frac{\Theta_l(s)}{\Theta_l^d(s)} = M(s)\frac{G_p(s,K,\upsilon)G_p^{-1}(s,0,0)+C(s)M(s)G_p(s,K,\upsilon)}{1+C(s)M(s)G_p(s,K,\upsilon)} \tag{71}$$

The magnitude at low frequencies is now higher than in the previous plot as consequence of the feedforward signal injected in θ_m^*. The magnitude is one at zero frequency in the free motion case, allowing for a good tracking of a tip position trajectory. In the contact motion cases, this magnitude is lower than one, but it is not relevant since the control system has switched to follow a force reference.

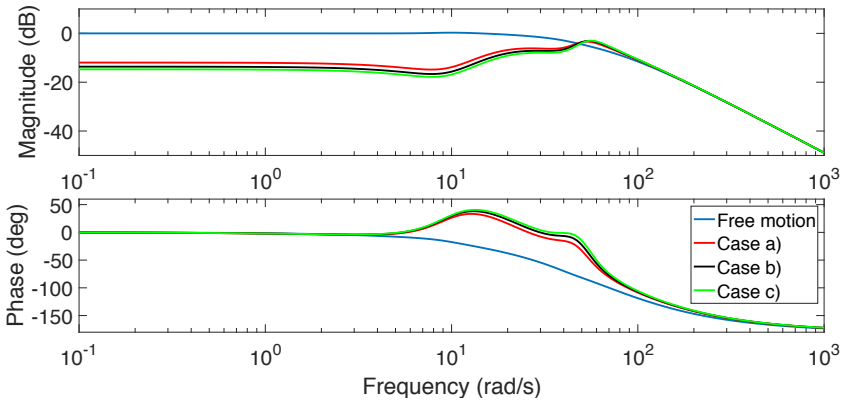

Figure 11: Bode diagrams of the closed-loop system (35) in the cases of free motion and constrained motion with the three mentioned impedances

Figure 12 depicts the gain crossover frequencies and the phase margins for the constrained motion cases of Table 3.

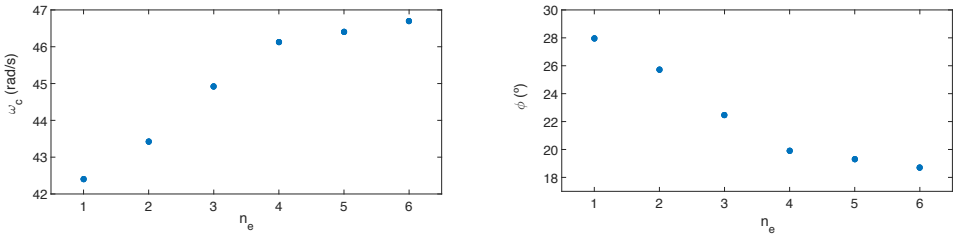

Figure 12: Frequency specifications attained by the robot in contact with the impedances of Table 3: (a) gain crossover frequency, (b) phase margin

4.5. Experimental Results

This section reports experiments carried out moving our flexible antenna in a controlled manner using the control scheme of Fig. 2 with controller (70). The angle of the tip of the link is controlled in the free movement and the force exerted by the link tip on the environment is controlled when it contacts an object. Three experiments were carried out: 1) free movement, 2) movement impacting with an object of variable impedance programming a torque reference $\Gamma_c^d = 0.1Nm$ and 3) movement impacting with an object of variable impedance programming a torque reference $\Gamma_c^d = 0.13Nm$. In the last two cases, the object was placed at the height of the antenna and in the middle of its horizontal trajectory, in such a way that the tip of the link impacted with the object. The initial location of the link and the location of the object did not change in all the experiments. Since Table 3 shows that the impedance of the environment changes in function of the exerted force (or the exerted coupling torque), two different coupling torque references were used to demonstrate the efficiency of our control system.

Figure 13 illustrates the results obtained for Experiment #1. In Fig. 13a, the reference of the angle of the tip $\theta_l^d(t)$, the reference modified by the prefilter $F(s) = M(s)$, $m(t) * \theta_l^d(t)$, the angle of the tip $\theta_l(t)$ and the angle of the motor $\theta_m(t)$ are represented. This figure shows that a good tracking of the trajectory of the flexible link tip is achieved. In fact, the tracking of the modified reference is quite accurate showing a tracking time delay of about 25 ms. This justifies the interest of applying Lemma 1. Figure 13b shows the reference of the coupling torque $\Gamma_c^d(t)$ and the coupling torque $\Gamma_c(t)$. This figure shows that the vibrations of the link are effectively removed.

Figure 14 shows the results of the experiment of the link impacting with our foam object having programmed a torque reference $\Gamma_c^d = 0.1Nm$ (Experiment #2), whereas Figure 15 shows the results of impacting the same object having programmed a torque reference $\Gamma_c^d = 0.13Nm$ (Experiment #3). These figures include plots of the reference of the tip angle, the motor and tip angles, and the coupling torque. It is remarked that the values of the torque references of Experiments #2 and #3 are included in the range of the Table 3, for which it was demonstrated that the closed-loop system fulfills the quadratic stability conditions for hybrid multiple systems. In both cases, a good trajectory tracking is observed until the link hits the object. At this moment, the im-

pact detection algorithm ([67]) detects the impact and the force control system starts to work. Figures 14 and 15 depict vertical dashed lines that separate the four stages of the methodology explained in the subsection 3.5.

Several positive aspects of the proposed control have been illustrated by these experiments:

1. The closed-loop system is robust to uncertainties and changes in the Coulomb and viscous friction of the motor. In particular, steady state errors caused by the Coulomb friction have been removed.

2. The impact detection algorithm performs adequately in both cases.

3. A good trajectory tracking of the tip of the link is obtained until the link impacts with the object.

4. A good force control is achieved after the impact has been detected, by using the methodology explained in 3.5.

5. The stage 4 of the force control methodology is necessary to make the error in the steady-state negligible.

6. The system is stable in all the cases. The experiments have therefore confirmed the stability of the system in free and constrained motion.

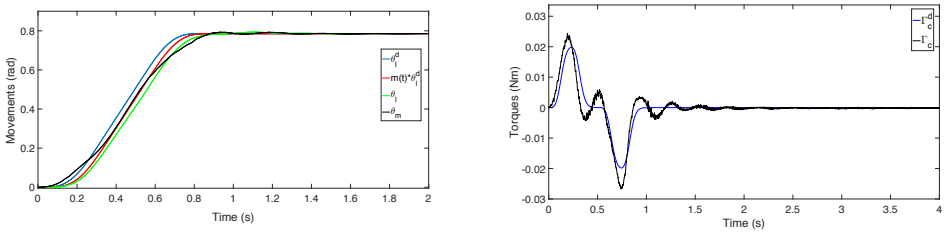

(a) (b)

Figure 13: Results for Experiment #1 (free motion): (a) angles, (b) torques

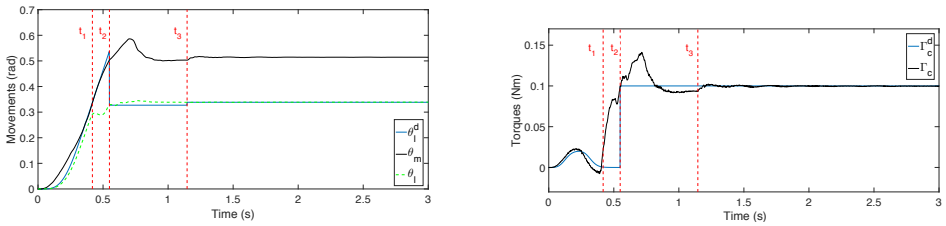

(a) (b)

Figure 14: Results for Experiment #2: (a) angles, (b) torques

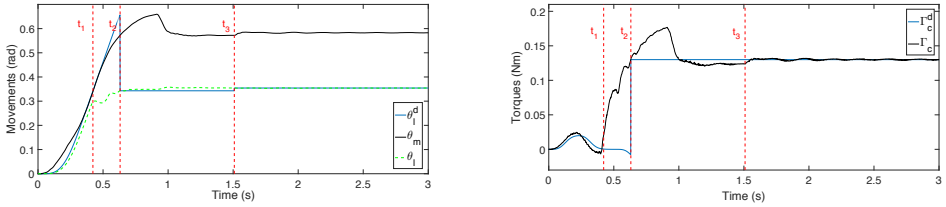

(a) (b)

Figure 15: Results for Experiment #3: (a) angles, (b) torques

4.6. Implementation of the fractional-order controller

Controller (70) has been implemented as follows. First, the error signal is passed through the low-pass filter $k_f/(1+\mu s)^2$ yielding an output signal $f(t)$. The fractional-order derivative operator s^α is subsequently applied to this signal yielding the output of the controller $y_c(t)$. Operator s^α is implemented using the following expression:

$$y_c(t) = T_s^{-\alpha} \sum_{n=0}^{N-1} (-1)^n \binom{\alpha}{n} f(t - nT_s) \tag{72}$$

where N is the number of terms involved in this discrete convolution, α is the fractional exponent, T_s is the sampling period and the combinatorial has been generalized in the following respect:

$$\binom{\beta}{l} = \frac{\beta(\beta+1)...(\beta-l+1)}{l!}. \tag{73}$$

Expression (72) has been obtained using the Grünwald-Letnikov (GL) definition of

the discretized fractional operators (e.g. [39]). Moreover, the short memory approximation described in [40] has been applied with N=500.

5. Conclusions

This paper has investigated the force control of a single-link flexible manipulator. Control of flexible robots is of interest in several applications like assembly tasks and collision minimization when the robot works with humans.

A fractional-order controller combined with a collision detection mechanism has been designed and implemented in order to accomplish five main control objectives: 1) the manipulator must exert a programmed force on the environment, 2) it must be robustly stable to uncertainties in the mechanical impedance of the contacted object, 3) efficient damping of vibrations must be attained in free and constrained movements (phase margin and gain crossover frequency have been used in this paper to assess this), 4) the control system must remain stable when transitions between free and constrained movements are produced (rebounds) and 5) the control system must remain stable when transitions among constrained movements with different mechanical impedances are produced.

All this has been achieved using the controller designed following the methodology proposed in Section 3. This methodology combines the obtention of a fractional-order robust controller to cope with unknown environment mechanical impedances with the fulfillment of some design conditions of hybrid fractional-order multimodel systems that guarantee the manipulator stability in the case of having rebounds or changes in the object impedance.

The proposed methodology has the advantage over other control methods of addressing by the first time the robust vibration damping control of flexible robots in contact with objects, besides guaranteeing stability to rebounds like in [22]. Experimental results show the effectiveness of the designed controller.

This article has demonstrated in Theorems 3 to 5 that the proposed D^{α} fractional-order controller has some advantages over standard *PD* controllers: it provides more phase margin, i.e, more damping and a higher gain crossover frequency, i.e, a faster

response in the cases of (a) free motion and (b) motion in contact with an object with a given stiffness K. It must be noticed that: 1) *PD* controllers are the ones for which robust asymptotic stability has been proven for flexible robots in the case of rebounds and 2) these are the controllers that have a similar degree of complexity as the D^{α} (two parameters to tune), then a fair comparison has been carried out in the theorems.

We mention that it is also the first time that the control of a robot that switches among free movement and movements constrained by an object with variable mechanical impedance has been studied. Previous works only addressed the problem of switching between free movement and movement contacting an object of constant but possibly unknown impedance (rebounds). We have considered here the case of an object whose impedance varies in function of the exerted force, and experiments of force control in this case have been provided.

The usual simplification that the contact is produced at the robot tip has been assumed in this paper. Our future work will consider the study of contact at any point of the link. Moreover, we plan to extend this strategy to a flexible link robot with several degrees of freedom.

Appendix A. Proof of Theorem 1

Condition (36) can be expressed as

$$\Re\left\{\left.\frac{H_{kd}(s)}{H_{ld}(s)}\right|_{s=j\omega}\right\}>0, \qquad \forall\omega \tag{A.1}$$

which, after substituting (35), (21) and (29) and operating subsequently yields

$$\Re\left\{\left.\frac{\left(s^2+\frac{\upsilon_0+\upsilon_k}{m}s+\frac{K_k}{m}+\omega_0^2\right)(1+\varepsilon s)^2 C_d(s)+\omega_0^2 C_n(s)}{\left(s^2+\frac{\upsilon_0+\upsilon_l}{m}s+\frac{K_l}{m}+\omega_0^2\right)(1+\varepsilon s)^2 C_d(s)+\omega_0^2 C_n(s)}\right|_{s=j\omega}\right\}>0, \qquad \forall\omega \tag{A.2}$$

Dividing the numerator and denominator of (A.2) by $(1+\varepsilon s)^2 C_d(s)$, substituting $s=s_n\omega_0$, defining the new parameters $K'_{\{i,k\}}=K_{\{i,k\}}/(m\omega_0^2)\geq 0$, $\upsilon'_{\{0,i,k\}}=\upsilon_{\{0,i,k\}}/(m\omega_0)\geq$

0 and $\varepsilon' = \varepsilon\omega_0$, denoting $X(s_n) = 1 + C(s_n)/(1+\varepsilon' s_n)^2$, and operating, it is obtained that

$$\Re\left\{ \left. \frac{s_n^2 + (\upsilon_0' + \upsilon_k')s_n + K_k' + X(s_n)}{s_n^2 + (\upsilon_0' + \upsilon_l')s_n + K_l' + X(s_n)} \right|_{s_n = j\omega_n} \right\} > 0, \qquad \forall \omega_n \tag{A.3}$$

where $\omega_n = \omega/\omega_0$. Particularizing $s_n = j\omega_n$ in (A.3), denoting $\Re\{X(j\omega_n)\} = X_r(\omega_n)$ and $\Im\{X(j\omega_n)\} = X_i(\omega_n)$, and operating yields condition (37). The proof of the theorem is completed.

Appendix B. Proof of Theorem 2

Proof. Consider any pair of models $H_l(s)$ and $H_k(s)$ that belong to the region. Their impedances, normalized according to Theorem 1, can be expressed as $K_l' = K_m' \pm \delta_K'$, $\upsilon_l' = \upsilon_m' \pm \delta_\upsilon'$ and $K_k' = K_m' \mp \delta_K'$, $\upsilon_k' = \upsilon_m' \mp \delta_\upsilon'$ being $K_m' = (K_l' + K_k')/2$, $\delta_K' = |K_l' - K_k'|/2$, $\upsilon_m' = (\upsilon_l' + \upsilon_k')/2$ and $\delta_\upsilon' = |\upsilon_l' - \upsilon_k'|/2$.

Substituting these expressions in condition (37) gives

$$\begin{aligned} &\left(\left(X_r(\omega_n) - \omega_n^2 + K_m'\right) \pm \delta_K'\right)\left(\left(X_r(\omega_n) - \omega_n^2 + K_m'\right) \mp \delta_K'\right) + \\ &\left(\left(X_i(\omega_n) + (\upsilon_0' + \upsilon_m')\omega_n\right) \pm \delta_\upsilon'\right)\left(\left(X_i(\omega_n) + (\upsilon_0' + \upsilon_m')\omega_n\right) \mp \delta_\upsilon'\right) > 0, \end{aligned} \tag{B.1}$$

$$0 \le \omega_n < \infty \tag{B.2}$$

which, after operating and rearranging terms, yields inequality (38).

It is self-apparent that K_m' and υ_m', which are the mean values of the stiffness and damping of the two systems, are always inside the intervals $\left(\frac{\underline{K}}{m\omega_0^2}, \frac{\overline{K}}{m\omega_0^2}\right)$ and $\left(\frac{\underline{\upsilon}}{m\omega_0}, \frac{\overline{\upsilon}}{m\omega_0}\right)$, respectively. It is also self-apparent that deviations of the two models with respect to the impedance mean values are always bounded by $\delta_K' \le \overline{\delta}_K'$ and $\delta_\upsilon' \le \overline{\delta}_\upsilon'$, being $\overline{\delta}_K' = min\left(K_m' - \frac{\underline{K}}{m\omega_0^2}, \frac{\overline{K}}{m\omega_0^2} - K_m'\right)$ and $\overline{\delta}_\upsilon' \le min\left(\upsilon_m' - \frac{\underline{\upsilon}}{m\omega_0}, \frac{\overline{\upsilon}}{m\omega_0} - \upsilon_m'\right)$.

Assume a pair of values K_m' and υ_m' and their corresponding maximum deviations $\overline{\delta}_K'$ and $\overline{\delta}_\upsilon'$. If inequality (38) was verified by these deviation values, it is self-apparent that the condition would also be verified by any smaller deviation values $\delta_K' \le \overline{\delta}_K'$ and/or $\delta_\upsilon' \le \overline{\delta}_\upsilon'$. Consequently, verification of (38) in all the range of mean values

(39) with the corresponding maximum deviations (40) implies its verification in all the range $\left(\underline{K},\overline{K}\right)$ and $(\underline{\upsilon},\overline{\upsilon})$. The proof of the theorem is completed.

Appendix C. Proof of Theorem 3

Frequency specifications have to fulfill the stability condition (48), which is independent of the form of the controller.

The closed-loop characteristic polynomial equation in the case of using (42) is

$$(1+\mu s)^2(1+\varepsilon s)^2\left(s^2+\frac{\upsilon_0}{m}s+\omega_0^2\right)+\omega_0^2(k_d s+k_p)=0 \tag{C.1}$$

whose independent term is $\omega_0^2+\omega_0^2 k_p$. A necessary condition for stability is that this term must be positive, which yields statement (54) of the theorem.

However, the closed-loop characteristic polynomial equation in the case of using (43) is

$$(1+\mu s)^2(1+\varepsilon s)^2\left(s^2+\frac{\upsilon_0}{m}s+\omega_0^2\right)+\omega_0^2 k_f s^\alpha=0 \tag{C.2}$$

whose independent term is ω_0^2, which is always positive. Then, in this case, an additional stability condition does not appear.

This difference can also be assessed from the inspection of the Nyquist plots of both control systems, which are shown in Fig. C.16. Fig. C.16a shows that $C_f(0)L(0)=0$. Then the only stability condition would be (48) if $C_f(s)$ were used. However, $C_i(0)L(0)=k_p$, and Fig. C.16b shows that the Nyquist plot surrounds the point $(-1,\ 0)$ in the case of using $C_i(s)$ if $k_p<-1$, being the closed-loop system unstable. The proof of the theorem is completed.

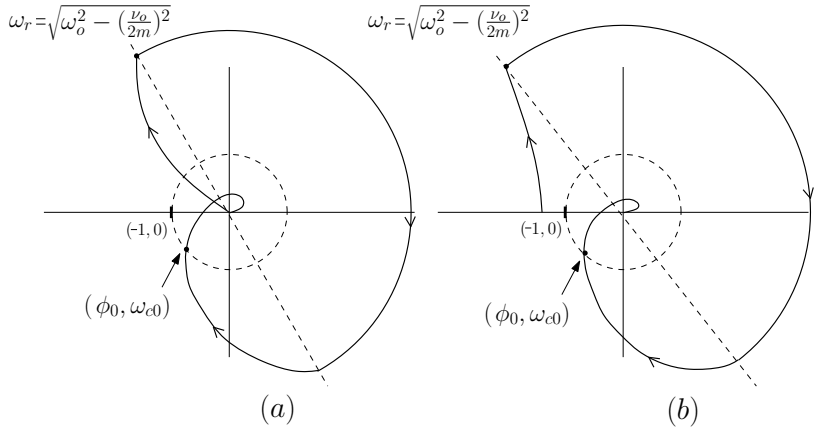

Figure C.16: First path of the Nyquist diagram of the robot using: (a) $C_f(s)$ with $\alpha > 1$ and (b) $C_i(s)$ with $k_p < 0$ ($k_p < -1$ in this case).

Appendix D. Proof of Lemma 4

The magnitude of the open-loop transfer function of the system with damping is

$$\left|G_p(j\omega,K,\upsilon)M(j\omega)C_i(j\omega)\right| = \frac{1}{1+\varepsilon^2\omega^2}\frac{1}{1+\mu^2\omega^2}\frac{\omega_0^2\sqrt{k_d^2\omega^2+k_p^2}}{\sqrt{\left(\omega_0^2+\frac{K}{m}-\omega^2\right)^2+\left(\frac{\upsilon_0+\upsilon}{m}\right)^2\omega^2}} \tag{D.1}$$

which has a gain crossover frequency ω_c. The magnitude of the open-loop transfer function of the same system without damping is

$$\left|G_p(j\omega,K,0)M(j\omega)C_i(j\omega)\right| = \frac{1}{1+\varepsilon^2\omega^2}\frac{1}{1+\mu^2\omega^2}\frac{\omega_0^2\sqrt{k_d^2\omega^2+k_p^2}}{\left|\omega_0^2+\frac{K}{m}-\omega^2\right|} \tag{D.2}$$

which has a gain crossover frequency ω_c'. Then both magnitudes can be related:

$$\begin{aligned}&\left|G_p(j\omega,K,\upsilon)M(j\omega)C_i(j\omega)\right| = \\ &\left|G_p(j\omega,K,0)M(j\omega)C_i(j\omega)\right|\frac{\left|\omega_0^2+\frac{K}{m}-\omega^2\right|}{\sqrt{\left(\omega_0^2+\frac{K}{m}-\omega^2\right)^2+\left(\frac{\upsilon_0+\upsilon}{m}\right)^2\omega^2}}\end{aligned} \tag{D.3}$$

Since $\left|G_p(j\omega_c,K,\upsilon)M(j\omega_c)C_i(j\omega_c)\right| = 1$ and $\frac{\left|\omega_0^2+\frac{K}{m}-\omega^2\right|}{\sqrt{\left(\omega_0^2+\frac{K}{m}-\omega^2\right)^2+\left(\frac{\upsilon_0+\upsilon}{m}\right)^2\omega^2}} < 1\ \forall\omega$ are verified, $\left|G_p(j\omega_c,K,0)M(j\omega_c)C_i(j\omega_c)\right|$ must therefore be higher than 1.

In expression (D.2), $1/\left(\left(1+\varepsilon^2\omega^2\right)\left(1+\mu^2\omega^2\right)\right)$ is a decreasing function. Moreover, it is subsequently demonstrated that $\frac{\omega_0^2\sqrt{k_d^2\omega^2+k_p^2}}{\left|\omega_0^2+\frac{K}{m}-\omega^2\right|}$ is also a decreasing function if $\omega > \sqrt{\omega_0^2+\frac{K}{m}}$. In this case, the derivative of this function with respect to ω is:

$$\frac{d}{d\omega}\left(\frac{\omega_0^2\sqrt{k_d^2\omega^2+k_p^2}}{\omega^2-\omega_0^2-\frac{K}{m}}\right) = -\frac{\omega_0^2\omega\left(k_d^2\left(\omega^2+\omega_0^2+\frac{K}{m}\right)+2k_p^2\right)}{\left(\omega^2-\omega_0^2-\frac{K}{m}\right)^2\sqrt{k_d^2\omega^2+k_p^2}} \tag{D.4}$$

which is apparent that is always negative and, then, this function is decreasing. Consequently, (D.2) is decreasing because it is the product of two decreasing functions and, since $\left|G_p(j\omega_c',K,0)M(j\omega_c')C_i(j\omega_c')\right| = 1$, ω_c must be lower than ω_c' in order to obtain that $\left|G_p(j\omega_c,K,0)M(j\omega_c)C_i(j\omega_c)\right| > 1$ (note that both ω_c and ω_c' are higher than $\sqrt{\omega_0^2+\frac{K}{m}}$ and (D.4) is therefore verified at these two frequencies). Then the first part of the lemma is proven.

The phase margin of the open-loop transfer function of the system with damping and a given K is

$$\begin{aligned}\phi = \pi + \angle G_p(j\omega_c,K,\upsilon)M(j\omega_c)C_i(j\omega_c) = \pi - 2arctan\left(\mu\omega_c\right)\\ -2arctan\left(\varepsilon\omega_c\right) + arctan\left(\frac{k_d\omega_c}{k_p}\right) - arctan\left(\frac{\frac{\upsilon_0+\upsilon}{m}\omega_c}{\omega_0^2+\frac{K}{m}-\omega_c^2}\right)\end{aligned} \tag{D.5}$$

The phase margin of the open-loop transfer function of the same system without damping and the same K is

$$\begin{aligned}\phi' = \pi + \angle G_p(j\omega_c',K,\upsilon)M(j\omega_c')C_i(j\omega_c') =\\ -2arctan\left(\mu\omega_c'\right) - 2arctan\left(\varepsilon\omega_c'\right) + arctan\left(\frac{k_d\omega_c'}{k_p}\right)\end{aligned} \tag{D.6}$$

The phase margin difference is

$$\phi-\phi' = 2\left(arctan\left(\mu\omega_c'\right)-arctan\left(\mu\omega_c\right)\right)+2\left(arctan\left(\varepsilon\omega_c'\right)-arctan\left(\varepsilon\omega_c\right)\right)+$$
$$\left(arctan\left(\frac{k_d\omega_c}{k_p}\right)-arctan\left(\frac{k_d\omega_c'}{k_p}\right)\right)+\pi-arctan\left(\frac{\frac{\upsilon_0+\upsilon}{m}\omega_c}{\omega_0^2+\frac{K}{m}-\omega_c^2}\right) \tag{D.7}$$

It is always verified that $\pi \geq arctan\left(\frac{\frac{\upsilon_0+\upsilon}{m}\omega_c}{\omega_0^2+\frac{K}{m}-\omega_c^2}\right)$. Since $\omega_c' > \omega_c$, it is verified that $arctan\left(\mu\omega_c'\right) > arctan\left(\mu\omega_c\right)$ and $arctan\left(\varepsilon\omega_c'\right) > arctan\left(\varepsilon\omega_c\right)$. Moreover, it is verified that $arctan\left(\frac{k_d\omega_c}{k_p}\right) > arctan\left(\frac{k_d\omega_c'}{k_p}\right)$ if $k_p < 0$ and $k_d > 0$. It is then apparent that $\phi-\phi' > 0$ and the second part of the lemma is proven.

Appendix E. Proof of Lemma 5

The magnitude of the open-loop transfer function of the system with damping is

$$\left|G_p(j\omega,K,\upsilon)M(j\omega)C_f(j\omega)\right| = \frac{1}{1+\varepsilon^2\omega^2}\frac{1}{1+\mu^2\omega^2}\frac{\omega_0^2 k_f\omega^\alpha}{\sqrt{\left(\omega_0^2+\frac{K}{m}-\omega^2\right)^2+\left(\frac{\upsilon_0+\upsilon}{m}\right)^2\omega^2}} \tag{E.1}$$

which has a gain crossover frequency ω_c. The magnitude of the open-loop transfer function of the same system without damping is

$$\left|G_p(j\omega,K,0)M(j\omega)C_f(j\omega)\right| = \frac{1}{1+\varepsilon^2\omega^2}\frac{1}{1+\mu^2\omega^2}\frac{\omega_0^2 k_f\omega^\alpha}{\left|\omega_0^2+\frac{K}{m}-\omega^2\right|} \tag{E.2}$$

which has a gain crossover frequency ω_c'. Then both magnitudes can be related:

$$\left|G_p(j\omega,K,\upsilon)M(j\omega)C_f(j\omega)\right| =$$
$$\left|G_p(j\omega,K,0)M(j\omega)C_f(j\omega)\right|\frac{\left|\omega_0^2+\frac{K}{m}-\omega^2\right|}{\sqrt{\left(\omega_0^2+\frac{K}{m}-\omega^2\right)^2+\left(\frac{\upsilon_0+\upsilon}{m}\right)^2\omega^2}} \tag{E.3}$$

Since $\left|G_p(j\omega_c,K,\upsilon)M(j\omega_c)C_f(j\omega_c)\right| = 1$ and $\frac{\left|\omega_0^2+\frac{K}{m}-\omega^2\right|}{\sqrt{\left(\omega_0^2+\frac{K}{m}-\omega^2\right)^2+\left(\frac{\upsilon_0+\upsilon}{m}\right)^2\omega^2}} < 1\ \forall\omega$ are verified, $\left|G_p(j\omega_c,K,0)M(j\omega_c)C_f(j\omega_c)\right|$ must therefore be higher than 1.

In expression (E.2), $1/\left(\left(1+\varepsilon^2\omega^2\right)\left(1+\mu^2\omega^2\right)\right)$ is a decreasing function. Moreover, it is subsequently demonstrated that $\frac{\omega_0^2 k_f \omega^\alpha}{\left|\omega_0^2+\frac{K}{m}-\omega^2\right|}$ is also a decreasing function if $\omega > \sqrt{\omega_0^2+\frac{K}{m}}$. In this case, the derivative of this function with respect to ω is:

$$\frac{d}{d\omega}\left(\frac{\omega_0^2 k_f \omega^\alpha}{\omega^2-\omega_0^2-\frac{K}{m}}\right) = -\omega_0^2\frac{k_f\omega^{\alpha-1}\left((2-\alpha)\right)\omega^2+\alpha\left(\omega_0^2+\frac{K}{m}\right)\right)}{\left(\omega^2-\omega_0^2-\frac{K}{m}\right)^2} \tag{E.4}$$

which is apparent that is always negative if $k_f > 0$ and $0 < \alpha < 2$ and, then, this function is decreasing. Consequently, (E.2) is decreasing because it is the product of two decreasing functions and, since $\left|G_p(j\omega_c',K,0)M(j\omega_c')C_f(j\omega_c')\right| = 1$, ω_c must be lower than ω_c' in order to obtain that $\left|G_p(j\omega_c,K,0)M(j\omega_c)C_f(j\omega_c)\right| > 1$ (note that both ω_c and ω_c' are higher than $\sqrt{\omega_0^2+\frac{K}{m}}$ and (E.4) is therefore verified at these two frequencies). Then the first part of the lemma is proven.

The phase margin of the open-loop transfer function of the system with damping and a given K is

$$\phi = \pi + \angle G_p(j\omega_c,K,\upsilon)M(j\omega_c)C_f(j\omega_c) =$$
$$\pi\left(1+\frac{\alpha}{2}\right) - 2arctan\left(\mu\omega_c\right) - 2arctan\left(\varepsilon\omega_c\right) - arctan\left(\frac{\frac{\upsilon_0+\upsilon}{m}\omega_c}{\omega_0^2+\frac{K}{m}-\omega_c^2}\right) \tag{E.5}$$

The phase margin of the open-loop transfer function of the same system without damping and the same K is

$$\phi' = \pi + \angle G_p(j\omega_c',K,\upsilon)M(j\omega_c')C_f(j\omega_c') = \frac{\pi}{2}\alpha - 2arctan\left(\mu\omega_c'\right) - 2arctan\left(\varepsilon\omega_c'\right) \tag{E.6}$$

The phase margin difference is

$$\phi-\phi'=2\left(arctan\left(\mu\omega_c'\right)-arctan\left(\mu\omega_c\right)\right)+2\left(arctan\left(\varepsilon\omega_c'\right)-arctan\left(\varepsilon\omega_c\right)\right)+\pi-arctan\left(\frac{\frac{\upsilon_0+\upsilon}{m}\omega_c}{\omega_0^2+\frac{K}{m}-\omega_c^2}\right) \tag{E.7}$$

It is always verified that $\pi \geq arctan\left(\frac{\frac{\upsilon_0+\upsilon}{m}\omega_c}{\omega_0^2+\frac{K}{m}-\omega_c^2}\right)$. Since $\omega_c' > \omega_c$, it is verified that $arctan\left(\mu\omega_c'\right) > arctan\left(\mu\omega_c\right)$ and $arctan\left(\varepsilon\omega_c'\right) > arctan\left(\varepsilon\omega_c\right)$. It is then apparent that $\phi-\phi' > 0$ and the second part of the lemma is proven.

Appendix F. Proof of Theorem 4

Assume that both $C_i(s)$ and $C_f(s)$ are designed to yield the same pair of frequency specifications. The gain crossover frequency ω_{ci} yielded using $C_i(s)$ verifies the condition

$$\frac{\omega_0^2 k_f \omega_{c0}^{\alpha}\sqrt{cos^2\left(\frac{\pi}{2}\alpha\right)\left(\frac{\omega_{ci}}{\omega_{c0}}\right)^2+sin^2\left(\frac{\pi}{2}\alpha\right)}}{\left|\omega_0^2+\frac{K}{m}-\omega_{ci}^2\right|}=1 \tag{F.1}$$

which is obtained by making $\varepsilon=\mu=0$, substituting parameters (53) in (D.2) and imposing that the value of this function must be 1. Taking into account that $\omega_{ci} > \sqrt{\omega_0^2+\frac{K}{m}}$ and solving for K in (F.1), it is obtained that

$$K=m\left(\omega_{ci}^2-\omega_0^2-\omega_0^2 k_f \omega_{c0}^{\alpha}\sqrt{cos^2\left(\frac{\pi}{2}\alpha\right)\left(\frac{\omega_{ci}}{\omega_{c0}}\right)^2+sin^2\left(\frac{\pi}{2}\alpha\right)}\right) \tag{F.2}$$

Let us denote the right-hand side of this expression as $f_i(\omega)$ so that $K=f_i(\omega_{ci})$.

The gain crossover frequency ω_{cf} yielded using $C_f(s)$ for the previous value of K verifies the condition

$$\frac{\omega_0^2 k_f \omega_{cf}^{\alpha}}{\left|\omega_0^2+\frac{K}{m}-\omega_{cf}^2\right|}=1 \tag{F.3}$$

which is obtained by making $\varepsilon = \mu = 0$ in (E.2) and imposing that the value of this function must be 1. Taking into account that $\omega_{cf} > \sqrt{\omega_0^2 + \frac{K}{m}}$ and solving for K in (F.3), it is obtained that

$$K = m\left(\omega_{cf}^2 - \omega_0^2 - \omega_0^2 k_f \omega_{cf}^{\alpha}\right) = f_f\left(\omega_{cf}\right) \tag{F.4}$$

Let us denote the right-hand side of this expression as $f_f(\omega)$ so that $K = f_f\left(\omega_{cf}\right)$.

For values $\omega > \omega_{c0}$, it is easily seen that

$$\begin{aligned}
\left(\frac{\omega}{\omega_{c0}}\right)^{\alpha} &< \sqrt{cos^2\left(\frac{\pi}{2}\alpha\right)\left(\frac{\omega}{\omega_{c0}}\right)^2 + sin^2\left(\frac{\pi}{2}\alpha\right)} \quad if \quad \alpha < 1 \\
\left(\frac{\omega}{\omega_{c0}}\right)^{\alpha} &> \sqrt{cos^2\left(\frac{\pi}{2}\alpha\right)\left(\frac{\omega}{\omega_{c0}}\right)^2 + sin^2\left(\frac{\pi}{2}\alpha\right)} \quad if \quad \alpha > 1
\end{aligned} \tag{F.5}$$

which implies that $f_f(\omega) > f_i(\omega)$ if $\alpha < 1$, and $f_f(\omega) < f_i(\omega)$ if $\alpha > 1$. Taking into account that $f_f(\omega)$ and $f_i(\omega)$ are bijective functions in the interval $\sqrt{\omega_0^2 + \frac{K}{m}} < \omega < \infty$, the previous result allows us to state that for a given stiffness value K: 1) if $\alpha < 1$ then $\omega_{cf} < \omega_{ci}$ and 2) if $\alpha > 1$ then $\omega_{cf} > \omega_{ci}$, which proves the results of the theorem about the gain crossover frequency.

The difference between the phase margins ϕ_i and ϕ_f, yielded using $C_i(s)$ and $C_f(s)$ respectively, is determined combining (D.6) and (E.6), making $\varepsilon = \mu = 0$ there, and operating. Taking into account that $k_d/k_p = tan\left(\frac{\pi}{2}\alpha\right)/\omega_{c0}$ and $arctan\left(tan\left(\frac{\pi}{2}\alpha\right)\frac{\omega_{ci}}{\omega_{c0}}\right) - \frac{\pi}{2}\alpha = arctan\left(\frac{tan\left(\frac{\pi}{2}\alpha\right)\left(\frac{\omega_{ci}}{\omega_{c0}}-1\right)}{1+tan^2\left(\frac{\pi}{2}\alpha\right)\frac{\omega_{ci}}{\omega_{c0}}}\right)$, it is obtained that

$$\phi_i - \phi_f = arctan\left(\frac{tan\left(\frac{\pi}{2}\alpha\right)\left(\frac{\omega_{ci}}{\omega_{c0}} - 1\right)}{1 + tan^2\left(\frac{\pi}{2}\alpha\right)\frac{\omega_{ci}}{\omega_{c0}}}\right) \tag{F.6}$$

Since always $\omega_{ci}/\omega_{c0} \geq 1$, it is apparent from this expression that $\phi_i - \phi_f > 0$ if $tan\left(\frac{\pi}{2}\alpha\right) > 0$, i.e., $0 < \alpha < 1$, and $\phi_i - \phi_f < 0$ if $tan\left(\frac{\pi}{2}\alpha\right) < 0$, i.e., $1 < \alpha < 2$, and the theorem has been proven.

Appendix G. Proof of Theorem 5

Assume that both $C_i(s)$ and $C_f(s)$ are designed to yield the same pair of frequency specifications (ϕ_0, ω_{c0}). Then relations (53) would hold.

The gain crossover frequency ω_{ci} yielded by $C_i(s)$ in the case of a stiffness $K > 0$ verifies the condition

$$\frac{1}{1+\varepsilon^2\omega_{ci}^2}\frac{\omega_0^2 k_f \omega_{c0}^{\alpha}\sqrt{cos^2\left(\frac{\pi}{2}\alpha\right)\left(\frac{\omega_{ci}}{\omega_{c0}}\right)^2 + sin^2\left(\frac{\pi}{2}\alpha\right)}}{\left|\omega_0^2+\frac{K}{m}-\omega_{ci}^2\right|} = 1 \tag{G.1}$$

which is obtained by substituting parameters (53) in (D.2), making $\mu = 0$ and imposing that the value of this function must be 1. Taking into account that $\omega_{ci} > \sqrt{\omega_0^2 + \frac{K}{m}}$ and solving for K in (G.1), it is obtained that

$$K = m\left(\omega_{ci}^2 - \omega_0^2 - \frac{\omega_0^2 k_f \omega_{c0}^{\alpha}}{1+\varepsilon^2\omega_{ci}^2}\sqrt{cos^2\left(\frac{\pi}{2}\alpha\right)\left(\frac{\omega_{ci}}{\omega_{c0}}\right)^2 + sin^2\left(\frac{\pi}{2}\alpha\right)}\right) = f_i(\omega_{ci}) \tag{G.2}$$

The gain crossover frequency ω_{cf} yielded by $C_f(s)$ for the previous K value verifies the condition

$$\frac{1}{1+\varepsilon^2\omega_{cf}^2}\frac{\omega_0^2 k_f \omega_{cf}^{\alpha}}{\left|\omega_0^2+\frac{K}{m}-\omega_{cf}^2\right|} = 1 \tag{G.3}$$

which is obtained by substituting parameters (53) in (E.2), making $\mu = 0$ and imposing that the value of this function must be 1. Taking into account that $\omega_{cf} > \sqrt{\omega_0^2 + \frac{K}{m}}$ and solving for K in (G.3), it is obtained that

$$K = m\left(\omega_{cf}^2 - \omega_0^2 - \frac{\omega_0^2 k_f \omega_{cf}^{\alpha}}{1+\varepsilon^2\omega_{cf}^2}\right) = f_f\left(\omega_{cf}\right) \tag{G.4}$$

For values $\omega > \omega_{c0}$, it is easily seen that

$$\left(\frac{\omega}{\omega_{c0}}\right)^{\alpha} > \sqrt{cos^2\left(\frac{\pi}{2}\alpha\right)\left(\frac{\omega}{\omega_{c0}}\right)^2 + sin^2\left(\frac{\pi}{2}\alpha\right)} \quad if \quad \alpha > 1 \tag{G.5}$$

which implies that $f_f(\omega) < f_i(\omega)$ if $\alpha > 1$. Taking into account that $f_f(\omega)$ and $f_i(\omega)$ are bijective functions in the interval $\sqrt{\omega_0^2 + \frac{K}{m}} < \omega < \infty$, the previous result allows us to state that, for a given stiffness value K, if $\alpha > 1$ then $\omega_{cf} > \omega_{ci}$. Then the first statement of the theorem has been proven.

Equation (G.4) can be expressed in terms of the new parameters defined in the theorem as

$$\left(\frac{\omega_0}{\omega_{c0}}\right)^2 + \frac{K}{m\omega_{c0}^2} = \left(\frac{\omega_{cf}}{\omega_{c0}}\right)^2 - \kappa \frac{\left(\frac{\omega_{cf}}{\omega_{c0}}\right)^\alpha}{1+\varsigma^2\left(\frac{\omega_{cf}}{\omega_{c0}}\right)^2} \tag{G.6}$$

Since (G.6) must be verified for all values $\omega_{cf} \geq \omega_{c0}$, making $\omega_{cf} = \omega_{c0}$ yields that

$$\left(\frac{\omega_0}{\omega_{c0}}\right)^2 + \frac{K}{m\omega_{c0}^2} = 1 - \frac{\kappa}{1+\varsigma^2} \tag{G.7}$$

and taking into account that $K \geq 0$ and operating, condition (64) is obtained.

Equating expressions (G.2) and (G.4) for a given stiffness K and introducing the new parameters yields

$$\left(\frac{\omega_{ci}}{\omega_{c0}}\right)^2 - \kappa \frac{\sqrt{cos^2\left(\frac{\pi}{2}\alpha\right)\left(\frac{\omega_{ci}}{\omega_{c0}}\right)^2 + sin^2\left(\frac{\pi}{2}\alpha\right)}}{1+\varsigma^2\left(\frac{\omega_{ci}}{\omega_{c0}}\right)^2} = \left(\frac{\omega_{cf}}{\omega_{c0}}\right)^2 - \kappa \frac{\left(\frac{\omega_{cf}}{\omega_{c0}}\right)^\alpha}{1+\varsigma^2\left(\frac{\omega_{cf}}{\omega_{c0}}\right)^2} \tag{G.8}$$

which defines the relation between ω_{ci} and ω_{cf} for the same value of K.

The difference between the phase margins ϕ_i and ϕ_f yielded for the same K using $C_i(s)$ and $C_f(s)$ respectively, is determined combining (D.6) and (E.6), making $\mu = 0$ and operating taking into account that $k_d/k_p = tan\left(\frac{\pi}{2}\alpha\right)/\omega_{c0}$, $arctan\left(tan\left(\frac{\pi}{2}\alpha\right)\frac{\omega_{ci}}{\omega_{c0}}\right) - \frac{\pi}{2}\alpha = arctan\left(\frac{tan\left(\frac{\pi}{2}\alpha\right)\left(\frac{\omega_{ci}}{\omega_{c0}}-1\right)}{1+tan^2\left(\frac{\pi}{2}\alpha\right)\frac{\omega_{ci}}{\omega_{c0}}}\right)$ and $arctan(\varepsilon\omega_{ci}) - arctan(\varepsilon\omega_{cf}) = arctan\left(\frac{\varepsilon(\omega_{ci}-\omega_{cf})}{1+\varepsilon^2\omega_{ci}\omega_{cf}}\right)$:

$$\phi_f - \phi_i = -arctan\left(\frac{tan\left(\frac{\pi}{2}\alpha\right)\left(\frac{\omega_{ci}}{\omega_{c0}}-1\right)}{1+tan^2\left(\frac{\pi}{2}\alpha\right)\left(\frac{\omega_{ci}}{\omega_{c0}}\right)}\right) - 2arctan\left(\frac{\varsigma\left(\frac{\omega_{cf}}{\omega_{c0}} - \frac{\omega_{ci}}{\omega_{c0}}\right)}{1+\varsigma^2\left(\frac{\omega_{ci}}{\omega_{c0}}\right)\left(\frac{\omega_{cf}}{\omega_{c0}}\right)}\right) \tag{G.9}$$

The regions for which $\phi_f - \phi_i \geq 0 \;\; \forall \omega_{cf} \geq \omega_{c0}$ have been calculated numerically from this expression for the ranges $0 < \varsigma \leq 1$, $0 < \kappa \leq 2$ and $1.05 \leq \alpha \leq 1.95$. The procedure has been:

1. For all the gain crossover frequencies $\omega_{cf} \geq \omega_{c0}$, the corresponding ω_{ci}, i.e., the gain crossover frequency ω_{ci} yielded by $C_i(s)$ for the same K that yielded ω_{cf} with $C_f(s)$, have been obtained from (G.8). This calculation is not difficult since it basically involves solving a fourth order polynomial for each ω_{cf}.
2. $\phi_f - \phi_i$ is calculated for each ω_{cf} by substituting this value and the before calculated ω_{ci} in (G.9). A point is included in the searched region if $\phi_f - \phi_i \geq 0 \;\forall \omega_{cf} \geq \omega_{c0}$, i.e., if this inequality is verified for all $K \geq 0$.
3. The border of the region obtained for a given α, $\kappa = h(\varsigma)$, is approximated by a fifth order polynomial.
4. The coefficients of the polynomials obtained for each α are approximated by fourth order polynomials in α.
5. Coefficients of the resulting matrix Ψ have been slightly modified in order to represent regions in which it is guaranteed that $\phi_f \geq \phi_i \;\forall \omega_{cf} \geq \omega_{c0}$.

And the last part of the theorem has been proven.

References

[1] V. Feliu, Robot flexibles: Hacia una generación de robots con nuevas prestaciones, Revista Iberoamericana de Automática e Informática Industrial 3 (2006) 24–41.

[2] I. Payo, V. Feliu, O. D. Cortázar, Force control of a very lightweight single-link flexible arm based on coupling torque feedback, Mechatronics 19 (2009) 334–347.

[3] A. Bicchi, G. Tonietti, Fast and "soft arm" tactics [robot arm design], IEEE Robotics and Automation Magazine 11 (2) (2004) 22–33.

[4] P. C. Watson, Remote center compliance system, US Patent 4,098,001 (Jul. 4 1978).

[5] D. E. Whitney, Historical perspective and state of the art in robot force control, The International Journal of Robotics Research 6 (1) (1987) 3–14.

[6] J. Versace, A review of the severity index, Tech. rep., SAE Technical Paper (1971).

[7] M. Benosman, G. L. Vey, Control of flexible manipulators: A survey, Robotica 22 (5) (2004) 533–545.

[8] N. Hogan, Impedance control: an approach to manipulation: Part I, II & III, Trans. ASME: J. Dynam. Syst., Meas., Control 107 (1985) 1–24.

[9] M. H. Raibert, J. J. Craig, Hybrid position/force control of manipulators, Journal of Dynamic Systems, Measurement, and Control 103 (2) (1981) 126–133.

[10] G. R. Vossoughi, A. Karimzadeh, Impedance control of a two degree-of-freedom planar flexible link manipulator using singular perturbation theory, Robotica 24 (02) (2006) 221–228.

[11] F. Matsuno, T. Asano, Y. Sakawa, Modeling and quasi-static hybrid position/force control of constrained planar two-link flexible manipulators, IEEE Transactions on Robotics and Automation 10 (3) (1994) 287–297.

[12] A. De Luca, R. Mattone, Sensorless robot collision detection and hybrid force/motion control, in: Robotics and Automation, 2005. ICRA 2005. Proceedings of the 2005 IEEE International Conference on, IEEE, 2005, pp. 999–1004.

[13] A. De Luca, A. Albu-Schaffer, S. Haddadin, G. Hirzinger, Collision detection and safe reaction with the DLR-III lightweight manipulator arm, in: Intelligent Robots and Systems, 2006 IEEE/RSJ International Conference on, IEEE, 2006, pp. 1623–1630.

[14] J. Malzahn, T. Bertram, Collision detection and reaction for a multi-elastic-link robot arm, IFAC Proceedings Volumes 47 (3) (2014) 320–325.

[15] T. Tarn, Y. Wu, N. Xi, A. Isidori, Force regulation and contact transition control, IEEE Control Systems 16 (1) (1996) 32–40.

[16] A. Garcia, V. Feliu, Force control of a single-link flexible robot based on a collision detection mechanism, IEE Proceedings-Control Theory and Applications 147 (6) (2000) 588–595.

[17] J. J. Craig, Introduction to robotics: Mechanics and Control, Vol. 3, Addison-Wesley, Reading-Massachusetts, 1986.

[18] A. Garcia, V. Feliu, J. A. Somolinos, Experimental testing of a gauge based collision detection mechanism for a new three-degree-of-freedom flexible robot, Journal of Field Robotics 20 (6) (2003) 271–284.

[19] J. Becedas, I. Payo, V. Feliu, Generalised proportional integral torque control for single-link flexible manipulators, IET Control Theory and Applications 4 (5) (2010) 773–783.

[20] J. Becedas, I. Payo, V. Feliu, Two-flexible-fingers gripper force feedback control system for its application as end effector on a 6-DOF manipulator, IEEE Transactions on Robotics 27 (3) (2011) 599–615.

[21] H. Zhao, C. D. Rahn, Repetitive learning control of a flexible whisker in tip contact with an unknown surface, Journal of Vibration and Control 17 (2) (2011) 197–203.

[22] F. Ching, D. Wang, Exact solution and infinite-dimensional stability analysis of a single flexible link in collision, IEEE Transactions on Robotics and Automation 19 (6) (2003) 1015–1020.

[23] S. Manabe, A suggestion of fractional-order controller for flexible spacecraft attitude control, Nonlinear Dynamics 29 (1) (2002) 251–268.

[24] D. Valério, J. S. da Costa, Fractional differentiation and its applications, LAPS, 2005, Ch. Fractional order control of a flexible robot, pp. 649–660.

[25] C. Monje, F. Ramos, V. Feliu, B. Vinagre, Tip position control of a lightweight flexible manipulator using a fractional order controller, IET Control Theory & Applications 1 (5) (2007) 1451–1460.

[26] G. W. Bohannan, Analog fractional order controller in temperature and motor control applications, Journal of Vibration and Control 14 (9-10) (2008) 1487–1498.

[27] N. M. Fonseca, J. A. T. Machado, Fractional-order hybrid control of robotic manipulators, in: Proceedings of the 11th International Conference on Advanced Robotics (ICAR'2003), 2003, pp. 393–398.

[28] N. M. F. Ferreira, J. A. T. Machado, J. K. Tar, Two cooperating manipulators with fractional controllers, International Journal of Advanced Robotic System 6 (4) (2009) 343–348.

[29] S. H. HosseinNia, I. Tejado, B. M. Vinagre, A method for the design of robust controllers ensuring the quadratic stability for switching systems, Journal of Vibration and Control 20 (7) (2014) 1085–1098.

[30] B. M. Vinagre, V. Feliu, I. Tejado, Fractional control: Fundamentals and user guide, Revista Iberoamericana de Automática e Informática Industrial 13 (3) (2016) 265–280.

[31] L. Meirovitch, Principles and techniques of vibrations, Vol. 1, Prentice Hall New Jersey, 1997.

[32] V. Feliu, F. Ramos, Strain gauge based control of single-link flexible very lightweight robots robust to payload changes, Mechatronics 15 (5) (2005) 547–571.

[33] V. Feliu, K. Rattan, H. Brown, Modelling and control of single-link flexible arms with lumped masses, ASME Journal of Dynamic Systems, Measurement, and Control 114 (1) (1992) 59–69.

[34] C. F. Castillo-Berrio, V. Feliu-Batlle, Vibration-free position control for a two degrees of freedom flexible-beam sensor, Mechatronics 27 (2015) 1–12.

[35] D. Feliu-Talegon, V. Feliu-Batlle, C. F. Castillo-Berrio, Motion control of a sensing antenna with a nonlinear input shaping technique, RIAI-Revista Iberoamericana de Automática e Informática Industrial 13 (2) (2016) 162–173.

[36] M. Kunze, A. Karimi, R. Longchamp, Frequency domain controller design by linear programming guaranteeing quadratic stability, in: Decision and Control, CDC 2008. Proceedings of the 47th IEEE International Conference on, IEEE, 2008, pp. 345–350.

[37] K. Ogata, Modern control engineering, Prentice Hall, EnglewoodCliffs, NewJersey, 1993.

[38] A. Piersol, J. Bendat, Engineering applications of correlation and spectral analysis, New York: Wiley Interscience, 1993.

[39] B. M. Vinagre, I. Podlubny, A. Hernandez, V. Feliu, Some approximations of fractional order operators used in control theory and applications, Fractional Calculus and Applied Analysis 3 (3) (2000) 231–248.

[40] I. Podlubny, Fractional differential equations, Vol. 198, Academic Press, 1998.